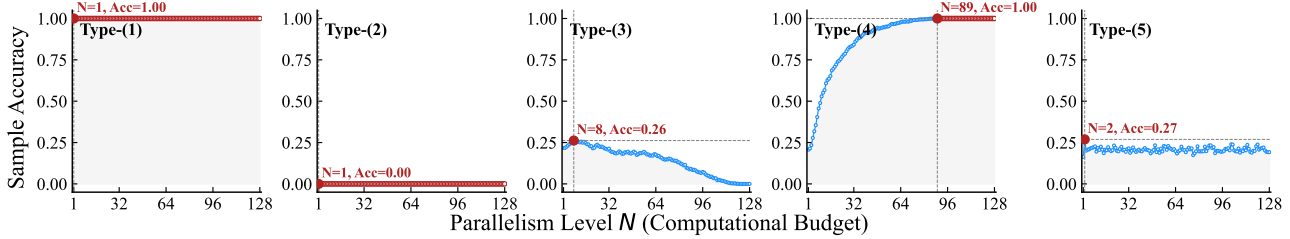
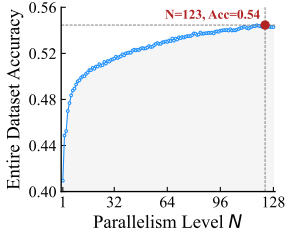


Breaking the Overscaling Curse: Thinking Parallelism Before Parallel Thinking

Yiming Wang¹ Zhuosheng Zhang¹ Rui Wang¹



↑ (i) **“Budget-Accuracy” Function for Individual Samples.** Samples are classified into five types based on the function monotonicity, including (1) Constant-1; (2) Constant-0; (3) *Approx.*-Decreasing; (4) *Approx.*-Increasing; (5) Non-monotonic (see Table 1 for details). Hollow red markers denote all points achieving the maximum accuracy, and the larger filled one highlights the smallest N attaining it.



← (ii) **“Budget-Accuracy” Function for the Entire Dataset.** Red marker indicates the best accuracy.

Figure 1. The Overscaling Curse of Parallel Thinking. When evaluating an entire dataset \mathcal{D} in a model, a large global parallelism level $N_{\mathcal{D}}$ is often used to maximize overall performance, as in *Episode (ii)*. Under this, as in *Episode (i)*, only type-(4) samples truly benefit, since they indeed require large N to realize substantial gains. In contrast, the other sample types do not benefit because they reach their best performance with only a small N . Therefore, *maximizing system-level efficacy usually introduces budget redundancy for some individual samples, i.e., reducing sample-level efficiency*. Examples here are from Qwen3-4B on the AIME25 dataset, with more shown in Appendix C.1 (Figure 6 - 17).

Abstract

Parallel thinking enhances LLM reasoning by multi-path sampling and aggregation. In system-level evaluations, a global parallelism level N is allocated to all samples, typically set large to maximize overall dataset accuracy. However, due to sample heterogeneity, some samples can achieve comparable performance with a smaller $N' < N$, causing budget redundancy. This incompatibility between system-level efficacy and sample-level efficiency constitutes the **overscaling curse**. In this paper, we formalize and quantify the overscaling curse, showing its universality and severity in practice, and analyze its trigger mechanism. We then propose a lightweight method, **T2**, to break the overscaling curse, which utilizes latent representations to estimate the optimal parallelism level for each sample before decoding. Experiments show that T2 significantly reduces cost while maintaining comparable performance, enabling more efficient parallel thinking.

¹School of Computer Science, Shanghai Jiao Tong University. Correspondence to: Yiming Wang <yiming.wang@sjtu.edu.cn>, Rui Wang <wangrui12@sjtu.edu.cn>.

Preprint.

1. Introduction

Large language models (LLMs) continually update their internal distributions during training on large-scale corpora (Vaswani, 2017; Brown et al., 2020), enabling them to encode broad world knowledge (Achiam et al., 2023) and exhibit strong reasoning abilities (Guo et al., 2025). As model capacity increases, recent work shows that model distributions contain latent information that is not fully revealed by standard autoregressive decoding (Chen et al., 2025b). This motivates scaling test-time computation (Snell et al., 2024; Muennighoff et al., 2025) to elicit models’ potential, a technique termed test-time scaling (TTS).

Among TTS, parallel thinking represents a distinct paradigm that broadens reasoning exploration (Fu et al., 2025; Zheng et al., 2025). During decoding, the model generates multiple *independent* reasoning paths in parallel through multinomial sampling (Hinton et al., 2015; Holtzman et al., 2019), which encourages diversity and broader coverage of the model’s output distribution. This paradigm typically pre-allocates a parallelism level $N \in \mathbb{N}^+$ and uses majority voting (Wang et al., 2022) to aggregate the N outputs into a final answer, where N serves as the computational budget.

When evaluating a model on a dataset, a global parallelism level N is applied to all samples. Under the TTS principle, which prioritizes performance over cost (Snell et al., 2024),

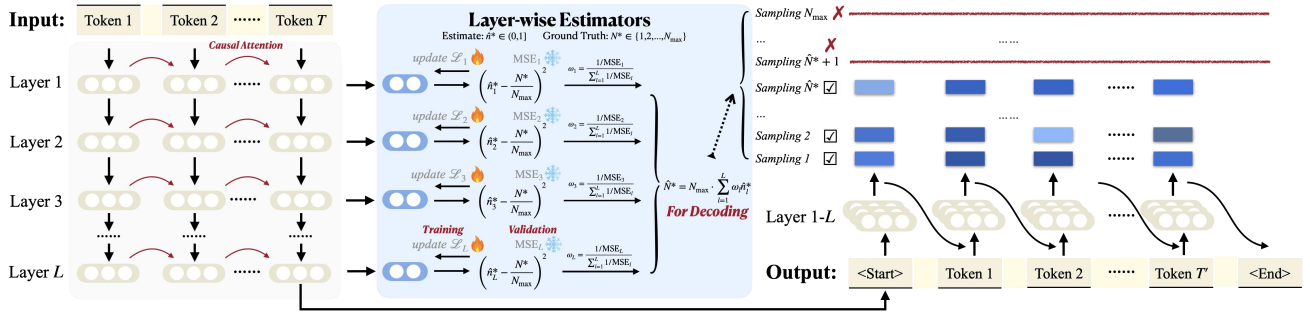


Figure 2. **T2: Thinking Parallelism Before Parallel Thinking.** We introduce trainable layer-wise estimators that predict the optimal parallelism level for each input from its final-token representations. These estimators are first trained, and each is assigned a weight based on its layer-wise validation error. During inference, after encoding the input, the layer-weighted parallelism estimate \hat{N}^* is obtained, and then decoding is performed under this budget. **T2 effectively breaks the overscaling curse and enables more efficient parallel thinking.**

N is chosen to maximize the overall dataset performance. For questions that are ambiguous to the given model, increasing N can improve accuracy by allowing additional sampling to converge to a more reliable decision. In contrast, for questions that are relatively easy or hard for that model, the outcome is less sensitive to additional sampling, so increasing N yields little or no gain. When such heterogeneous samples coexist, N is driven upward to exploit the gains on ambiguous samples, but this induces redundant computation on the rest, which can achieve comparable accuracy with much smaller $N' < N$. Such sample heterogeneity is common in practice. Therefore, an *incompatibility* emerges between *system-level efficacy* and *sample-level efficiency*: maximizing the dataset performance usually incurs budget redundancy on some individual samples. We term this the **overscaling curse** (see Figure 1 for illustration).

In this paper, we make two main progressive contributions:

- **Analyze Overscaling Curse:** We first define the overscaling curse from a macro budget redundancy perspective (Section 3.1) and introduce a quantitative metric, demonstrating its universality and severity across diverse models and datasets (Section 3.2). Further, following the intuition in Figure 1, we analyze its triggering mechanism from a micro sample heterogeneity perspective, and figure out why overscaling usually arises in practice (Section 3.3).
- **Break Overscaling Curse:** We introduce trainable layer-wise estimators that probe latent input representations to predict the sample-optimal parallelism level, achieving great estimation performance (Section 4.1). Building on this, we propose T2 (see Figure 2 for detailed pipeline), which inserts these estimators before decoding: for each input, it first obtains a parallelism estimate, and then allocates the decoding budget according to this estimate (Section 4.2). Experiments show that T2 substantially reduces inference latency and memory overhead compared to standard parallel thinking and prior adaptive-budget methods, while maintaining comparable performance (Section 5).

2. Preliminary

2.1. Parallel Thinking

We adopt the most common and standard definition of *parallel thinking* from Fu et al. (2025); Zeng et al. (2025). Let $\pi_\theta(\mathbf{y}|\mathbf{x})$ be an autoregressive language model that generates an output sequence $\mathbf{y} = (y_1, \dots, y_{T'})$ conditioned on an input sequence $\mathbf{x} = (x_1, \dots, x_T)$, where $y_t \sim \pi_\theta(\cdot | \mathbf{x}, \mathbf{y}_{<t})$. Sampling decoding typically employs multinomial sampling strategies, such as top- k (Fan et al., 2018) and top- p (Holtzman et al., 2019) sampling, to promote output diversity. Parallel thinking independently samples N reasoning paths $\{\mathbf{y}^i\}_{i=1}^N$ under these strategies, and selects the final one via unsupervised majority voting (Wang et al., 2022).

2.2. Global Experimental Setup

Language Model. We use four models: Qwen2.5-7B, Llama3.1-8B, Deepseek-R1-Distill-Qwen-7B, and Qwen3-4B. The first two are non-reasoning models, the third is a reasoning model, and the last one, while categorized as a non-reasoning model (we use Instruct-2507 version here), exhibits strong reasoning ability in practice. **They together provide a broad diversity of series and paradigms for our study.** Full citations are in Appendix D.

Dataset. We use six datasets: MATH500 (Hendrycks et al., 2021), AMC (MAA), AIME24 (MAA, 2024), AIME25 (MAA, 2025), GPQA (Rein et al., 2024), MMLU-Pro (Wang et al., 2024c). The first four are from the mathematical domain, with their difficulties increasing progressively. The last two cover other domains such as physics, linguistics, and world knowledge. **They together provide a broad diversity of task difficulty and domains for our study.**

Implementation. We conduct multinomial sampling with combined top- k , top- p , and temperature T strategies. Following Yang et al. (2025a); Guo et al. (2025), we set $k = 20$, $p = 0.95$, and $T = 0.6$ unless otherwise specified. Sampling is implemented with the Python `vLLM` library’s `model.generate()` function with full hardware parallelization. All experiments are run on 80G A100 GPUs.

2.3. “Budget-Accuracy” Function for Each Sample

In standard evaluations, performance is measured at the system level. Given a dataset \mathcal{D} with underlying distribution $P_{\mathcal{D}}$ and $(\mathbf{x}, \mathbf{y}) \sim P_{\mathcal{D}}$, where \mathbf{x} and \mathbf{y} denote the question and the ground-truth answer, the model is evaluated over R independent runs to reduce randomness (Guo et al., 2025). At parallelism level N , in each run r the model generates N candidate answers $\mathcal{A}_{\mathbf{x},N}^r = \{\mathbf{a}_{\mathbf{x},n}^r\}_{n=1}^N$ for each input \mathbf{x} , which are then aggregated by majority voting. Averaging correctness over all samples and runs yields the dataset accuracy $A_{\mathcal{D}}(N)$. By exchanging the order of expectations, $A_{\mathcal{D}}(N)$ equals the average of **sample accuracy** $A_{\mathbf{x}}(N)$:

$$\begin{aligned} A_{\mathcal{D}}(N) &= \mathbb{E}_{r \sim [R]} \mathbb{E}_{(\mathbf{x}, \mathbf{y}) \sim P_{\mathcal{D}}} \left[\mathbb{I}(f(\{\mathbf{a}_{\mathbf{x},n}^r\}_{n=1}^N) = \mathbf{y}) \right] \\ &= \mathbb{E}_{(\mathbf{x}, \mathbf{y}) \sim P_{\mathcal{D}}} \underbrace{\mathbb{E}_{r \sim [R]} \left[\mathbb{I}(f(\{\mathbf{a}_{\mathbf{x},n}^r\}_{n=1}^N) = \mathbf{y}) \right]}_{A_{\mathbf{x}}(N)}. \end{aligned} \quad (1)$$

Ideally, $A_{\mathbf{x}}(N)$ is an expectation that should be estimated via large-scale runs. However, such repeated sampling is computationally expensive under limited resources. To efficiently estimate it, we adopt a subsampling as follows.

Definition 2.1. For input \mathbf{x} , we first generate a reference set of N_{\max} outputs¹ $\mathcal{A}_{\mathbf{x},N_{\max}} = \{\mathbf{a}_{\mathbf{x},n}\}_{n=1}^{N_{\max}}$. For any $N \in [1, N_{\max}]$, we uniformly select N outputs without replacement from $\mathcal{A}_{\mathbf{x},N_{\max}}$ and determine correctness via majority voting. Repeating this subsampling M times yields:

$$\begin{aligned} A_{\mathbf{x}}(N) &= \mathbb{E}_{m \sim [M]} \left[\mathbb{I}(f(\{\mathbf{a}_{\mathbf{x},n}^m\}_{n=1}^N) = \mathbf{y}) \right], \\ \text{where } M &= \min \left\{ \tau, \binom{N_{\max}}{N} \right\} \\ \{\mathbf{a}_{\mathbf{x},n}^m\}_{n=1}^N &\sim \text{Uniform}_{\text{w/o repl.}}(\mathcal{A}_{\mathbf{x},N_{\max}}, N), \end{aligned} \quad (2)$$

with τ being a predefined large threshold² to prevent unbounded combinatorial enumeration.

Without subsampling, limited computational resources permit only a small number R of independent runs. With subsampling, a single large run suffices, which we reuse via M combinatorial samplings, reducing cost while improving the precision of estimating $A_{\mathbf{x}}(N)$. Using Eq.2, we compute $A_{\mathbf{x}}(N)$ for each N , obtaining a discrete “budget-accuracy” function $A_{\mathbf{x}} : \{1, \dots, N_{\max}\} \rightarrow [0, 1]$ for each sample.

3. Overscaling Curse of Parallel Thinking

3.1. What is the Overscaling Curse?

According to the TTS principle of parallel thinking, which prioritizes accuracy over cost (Snell et al., 2024), the goal is

¹We set $N_{\max} = 128$ in all subsequent experiments. To prioritize performance under the TTS principle, we double N by doubling from 2 to 2^7 until accuracy saturates for nearly all samples, ensuring performance convergence before efficiency analysis.

²We set the large threshold $\tau = 10^5$, yielding p -values below 0.01 in all subsequent experiments.

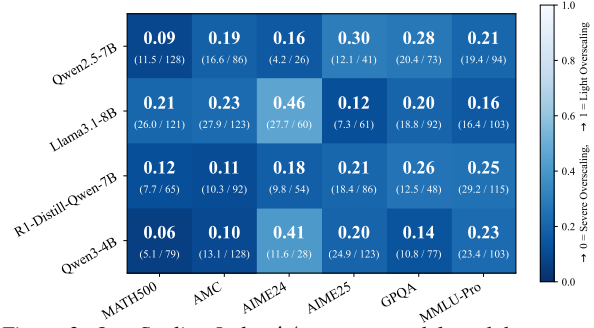


Figure 3. *OverScaling Index* $\mathcal{M}_{\mathcal{D}}$ across models and datasets, with detailed $(N_{\mathcal{D}}^*/N_{\mathcal{D}})$ labeled below each value.

first to maximize performance regardless of computational cost and then to choose the smallest N that attains this maximum to minimize redundancy. Therefore, for a sample $(\mathbf{x}, \mathbf{y}) \sim P_{\mathcal{D}}$, its **sample-optimal parallelism level** $N_{\mathbf{x}}^*$ is

$$N_{\mathbf{x}}^* = \min \left(\underset{N \in [1, N_{\max}]}{\operatorname{argmax}} [A_{\mathbf{x}}(N)] \right). \quad (3)$$

We denote $N_{\mathcal{D}}^* = \mathbb{E}_{(\mathbf{x}, \mathbf{y}) \sim P_{\mathcal{D}}} [N_{\mathbf{x}}^*]$ as the average $N_{\mathbf{x}}^*$ over \mathcal{D} . Similarly, for the entire dataset, its overall performance under N can be denoted as $\mathbb{E}_{(\mathbf{x}, \mathbf{y}) \sim P_{\mathcal{D}}} [A_{\mathbf{x}}(N)]$. Accordingly, the **system-optimal parallelism level** $N_{\mathcal{D}}$ is

$$N_{\mathcal{D}} = \min \left(\underset{N \in [1, N_{\max}]}{\operatorname{argmax}} \mathbb{E}_{(\mathbf{x}, \mathbf{y}) \sim P_{\mathcal{D}}} [A_{\mathbf{x}}(N)] \right). \quad (4)$$

Definition 3.1 (Overscaling Curse). The essence of overscaling is that maximizing overall dataset performance usually introduces budget redundancy for some individual samples. This can be formalized as $N_{\mathcal{D}} > N_{\mathcal{D}}^*$, i.e.,

$$\begin{aligned} &\min \left(\underset{N \in [1, N_{\max}]}{\operatorname{argmax}} \mathbb{E}_{(\mathbf{x}, \mathbf{y}) \sim P_{\mathcal{D}}} [A_{\mathbf{x}}(N)] \right) \\ &> \mathbb{E}_{(\mathbf{x}, \mathbf{y}) \sim P_{\mathcal{D}}} \min \left(\underset{N \in [1, N_{\max}]}{\operatorname{argmax}} [A_{\mathbf{x}}(N)] \right) \end{aligned} \quad (5)$$

3.2. How Severe Is the Overscaling Curse?

Based on Def.3.1, we first quantify the overscaling curse.

Definition 3.2 (Overscaling Index $\mathcal{M}_{\mathcal{D}}$). When evaluating the dataset \mathcal{D} using a single model, $\mathcal{M}_{\mathcal{D}}$ measures the degree of budget redundancy for individual samples when the dataset performance is maximized:

$$\mathcal{M}_{\mathcal{D}} = \frac{N_{\mathcal{D}}}{N_{\mathcal{D}}^*}, \quad (6)$$

We have $\mathcal{M}_{\mathcal{D}} \in [\frac{1}{N_{\max}}, N_{\max}]$. When $\mathcal{M}_{\mathcal{D}} < 1$ (e.g., $\mathcal{M}_{\mathcal{D}} = 0.2$), it implies that 80% of the budget is wasted. Thus, smaller values indicate more severe overscaling, whereas values closer to one indicate milder overscaling. When $\mathcal{M}_{\mathcal{D}} \geq 1$, overscaling is absent. Figure 3 reports $\mathcal{M}_{\mathcal{D}}$ across models and datasets. We observe that all $\mathcal{M}_{\mathcal{D}} < 1$, indicating that the overscaling curse is universal. Furthermore, none of the $\mathcal{M}_{\mathcal{D}}$ values exceed 0.5, implying that at least 50% of the budget is redundant across all evaluation groups. Notably, 11 out of 24 groups even have $\mathcal{M}_{\mathcal{D}} < 0.2$,

Table 1. Five sample types partition the dataset \mathcal{D} according to the monotonicity of $A_{\mathbf{x}}(N)$, where $\bigcap_{i=1}^5 \mathcal{D}_i = \emptyset$ and $\bigcup_{i=1}^5 \mathcal{D}_i = \mathcal{D}$. We can interpret these types from the perspective of the answer distribution, with details provided in Appendix B.1.

Type ID	Subset	$A_{\mathbf{x}}(N)$ Monotonicity	Sample Feature
1	\mathcal{D}_1	$A_{\mathbf{x}}(N) \equiv 1$	The model always answers correctly.
2	\mathcal{D}_2	$A_{\mathbf{x}}(N) \equiv 0$	The model always answers incorrectly.
3	\mathcal{D}_3	$A_{\mathbf{x}}(N) \approx_{-1} \text{mono}$ but $A_{\mathbf{x}}(N) \not\equiv 1$ or 0	The model produces the correct answer relatively infrequently, increasing N allows incorrect answers to dominate, making the correct answer less likely to be selected.
4	\mathcal{D}_4	$A_{\mathbf{x}}(N) \approx_{+1} \text{mono}$ but $A_{\mathbf{x}}(N) \not\equiv 1$ or 0	The model produces the correct answer relatively frequently, increasing N allows correct answer to dominate, making the correct answer easier to be selected.
5	\mathcal{D}_5	No Clear Monotonicity	Neither of the above is satisfied, indicating that as N increases, the answer distribution remains relatively uniform.

Table 2. $N_{\mathcal{D}_i}^*$ and $\Delta_{\mathcal{D}_i}$ of each subset \mathcal{D}_i across datasets \mathcal{D} for Qwen3-4B. Results of other models are in Appendix C.2.

\mathcal{D}	$N_{\mathcal{D}_i}^*$					$\Delta_{\mathcal{D}_i}(1, N_{\mathcal{D}_i}^*)$					$\Delta_{\mathcal{D}_i}(N_{\mathcal{D}_i}^*, N_{\max})$				
	(1)	(2)	(3)	(4)	(5)	(1)	(2)	(3)	(4)	(5)	(1)	(2)	(3)	(4)	(5)
MATH500	1.0	1.0	4.3	14.6	21.2	0.0	0.0	-0.12	0.18	0.03	0.0	0.0	-0.00	0.03	0.00
AMC	1.0	1.0	1.3	42.1	24.1	0.0	0.0	-0.03	0.24	0.03	0.0	0.0	-0.01	0.06	0.02
AIME24	1.0	1.0	5.5	16.2	9.9	0.0	0.0	-0.12	0.23	-0.02	0.0	0.0	-0.02	0.05	0.00
AIME25	1.0	1.0	2.7	51.7	2.0	0.0	0.0	-0.03	0.31	0.00	0.0	0.0	-0.01	0.05	0.01
GPQA	1.0	1.0	3.3	46.7	8.2	0.0	0.0	-0.04	0.30	0.00	0.0	0.0	-0.01	0.06	0.01
MMLU-Pro	1.0	1.0	6.1	39.9	6.7	0.0	0.0	-0.10	0.32	-0.01	0.0	0.0	-0.03	0.04	-0.01

meaning that over 80% of the budget is wasted in nearly half of the cases. These results demonstrate **both the universality and severity of the overscaling curse in practice**.

3.3. Why the Overscaling Curse Arises?

After establishing the universality of the overscaling curse, we further analyze its triggering mechanism following the intuition in Figure 1. From the perspective of sample heterogeneity, we formally classify samples by the monotonicity of their $A_{\mathbf{x}}(N)$ functions as follows:

Definition 3.3 (Approximate Monotonicity of $A_{\mathbf{x}}(N)$). Let $s := \lfloor \sqrt{N_{\max}} \rfloor$ be the step size for monotonicity checking. For $\alpha \in \{+1, -1\}$, $A_{\mathbf{x}}(N)$ is *approximately monotone* in direction α , denoted by $A_{\mathbf{x}}(N) \approx_{\alpha} \text{mono}$, iff.

$$\sum_{i=1}^{N_{\max}-s} \frac{\mathbb{I}\{\alpha(A_{\mathbf{x}}(i+s) - A_{\mathbf{x}}(i)) >= 0\}}{N_{\max} - s} \geq 0.80. \quad (7)$$

$A_{\mathbf{x}}(N) \approx_{+1} \text{mono}$ denotes approximately increasing, and $A_{\mathbf{x}}(N) \approx_{-1} \text{mono}$ denotes approximately decreasing.

Based on this property, samples can be grouped into five types in Table 1, with examples shown in Figure 1(i).

We focus on two features of these sample types in practice: the *sample-optimal parallelism level* and the *performance gain*. The former is defined in Eq. 3. For the latter, we define the performance gain for input \mathbf{x} over $[N_1, N_2]$ as

$$\Delta_{\mathbf{x}}(N_1, N_2) = A_{\mathbf{x}}(N_2) - A_{\mathbf{x}}(N_1), \quad (8)$$

and $\Delta_{\mathcal{D}_i}(N_1, N_2) = \mathbb{E}_{(\mathbf{x}, \mathbf{y}) \sim P_{\mathcal{D}_i}} [\Delta_{\mathbf{x}}(N_1, N_2)]$ is the average gain over \mathcal{D}_i . The value of $\mathcal{M}_{\mathcal{D}}$ is jointly determined by $N_{\mathcal{D}}^*$ and $N_{\mathcal{D}}$. Let $p_i := \mathbb{P}_{(\mathbf{x}, \mathbf{y}) \sim P_{\mathcal{D}}}[\mathbf{x} \in \mathcal{D}_i]$ denote the proportion of type- (i) samples in \mathcal{D} , then $N_{\mathcal{D}}^*$ can be rewritten as $N_{\mathcal{D}}^* = \sum_{i=1}^5 p_i N_{\mathcal{D}_i}^*$, so that $N_{\mathcal{D}_i}^*$ is important to determine $N_{\mathcal{D}}^*$. In addition, since $A_{\mathbf{x}}(N) = A_{\mathbf{x}}(1) + \Delta_{\mathbf{x}}(1, N)$, $N_{\mathcal{D}}$ can be rewritten as $N_{\mathcal{D}} = \min\left(\arg\max_{N \in [1, N_{\max}]} \sum_{i=1}^5 p_i \Delta_{\mathcal{D}_i}(1, N)\right)$, so that $\Delta_{\mathcal{D}_i}$ is important to determine $N_{\mathcal{D}}$.

The left part of Table 2 reports $N_{\mathcal{D}_i}^*$ values for each \mathcal{D}_i . For type-(1) and -(2), $N_{\mathbf{x}}^* \equiv 1$, so any $N_{\mathcal{D}} > 1$ incurs pure budget redundancy. Type-(3) and -(4) have opposite monotonicity, making $N_{\mathcal{D}_3}^*$ small (slightly above 1), while $N_{\mathcal{D}_4}^*$ much larger, often in the tens. Type-(5) behaves like noise, with $N_{\mathcal{D}_5}^*$ showing irregular patterns across datasets, but is largely smaller than $N_{\mathcal{D}_4}^*$. Overall, only type-(4) indeed benefits from large N , while the other types do not.

The right part of Table 2 reports $\Delta_{\mathcal{D}_i}$ with $N_{\mathcal{D}_i}^*$ as a boundary. For type-(1) and -(2), $\Delta_{\mathcal{D}_i} \equiv 0$, so they do not affect dataset performance. Type-(5) also has $\Delta_{\mathcal{D}_5} \approx 0$; its non-monotonic behavior yields fluctuating accuracy and negligible contribution. In contrast, type-(3) and -(4) dominate. Before $N_{\mathcal{D}_4}^*$, the positive gain of type-(4) $\Delta_{\mathcal{D}_4}$ substantially compensates for the negative gain of type-(3) $\Delta_{\mathcal{D}_3}$, and type-(3) exhibits negligible contribution beyond $N_{\mathcal{D}_4}^*$.

Under these findings, we can intuitively conclude that type-(4) samples are key to triggering the overscaling curse. When they coexist with other types, $N_{\mathcal{D}}$ is pulled toward the large $N_{\mathcal{D}_4}^*$ to exploit large gains of type-(4), therefore inducing redundancy for other sample types with much smaller $N_{\mathcal{D}_i}^*$. To formalize this effect, we derive a lower bound on $\mathcal{M}_{\mathcal{D}}$ with p_4 as the varying parameter, showing that such coexistence is the dominant driver of overscaling.

Theorem 3.4. Let $\kappa = N_{\mathcal{D}_3}^* + N_{\mathcal{D}_5}^* - 1$, and

$$\delta := \inf_{1 \leq N \leq N_{\mathcal{D}_4}^*} \frac{\Delta_{\mathcal{D}_4}(N, N_{\mathcal{D}_4}^*)}{-\Delta_{\mathcal{D}_3}(N, N_{\mathcal{D}_4}^*)}, \quad (9)$$

then $\mathcal{M}_{\mathcal{D}}$ satisfies:

$$\mathcal{M}_{\mathcal{D}} \leq \varphi(p_4) := \frac{\kappa + p_4(N_{\mathcal{D}_4}^* - \kappa)}{1 + (N_{\mathcal{D}_4}^* - 1) \mathbf{1}\{p_4 \delta > 1 - p_4\}}. \quad (10)$$

See Appendix B.2 for the proof. δ is typically large because the positive gains of type-(4) dominate the negative gains of type-(3), resulting in a low activation threshold $\frac{1}{1+\delta}$. This theorem implies for any $p_4 \in (\frac{1}{1+\delta}, 1)$, $\varphi(p_4) < 1$ and decreases as p_4 moves away from 1. Consequently, **when p_4 lies away from both 0 and 1, the overscaling curse is more likely to be triggered, and its severity increases as p_4 decreases, except in the limit $p_4 \rightarrow 0$** . At the two endpoints, when $p_4 = 0$, \mathcal{D} contains no type-(4) samples and $N_{\mathcal{D}}$ is driven toward smaller values near $N_{\mathcal{D}_i}^*$ ($i \neq 4$), reducing redundancy. When $p_4 = 1$, \mathcal{D} consists solely of type-(4) samples, though $N_{\mathcal{D}}$ shifts toward large values near $N_{\mathcal{D}_4}^*$, no cross-type redundancy arises.

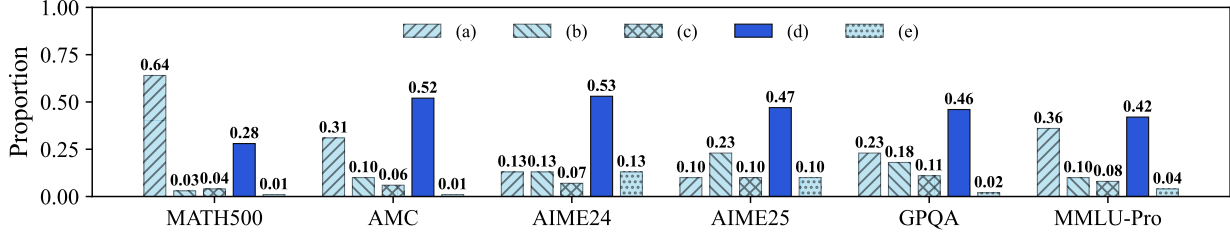


Figure 4. Proportion of the five sample types across datasets in Qwen3-4B. Results of other models are shown in Appendix C.3.

Figure 4 reports the proportions $\{p_i\}_{i=1}^5$ of the five sample types in practice. We observe that p_4 typically lies between 0.2 and 0.6. Being far from 0 or 1, this regime falls into the range where the overscaling curse is more likely to be triggered. These results corroborate our theoretical analysis that the coexistence of type-(4) samples with other types is a dominant driver of overscaling in practice.

4. Breaking the Overscaling Curse

In this section, we study how to break the overscaling curse under system-level evaluation. Since the dataset distribution is fixed, we cannot exclude or contain only type-(4) samples for it. Thus, the most feasible way to reduce budget redundancy is to replace the global $N_{\mathcal{D}}$ with the sample-specific $N_{\mathbf{x}}^*$ (Eq.3). As $N_{\mathbf{x}}^*$ is unknown in practice, we estimate it by probing latent input representations before decoding.

4.1. Thinking Parallelism via Latent Inputs

Task Setup. A language model consists of L Transformer decoder layers. Given an input $\mathbf{x} = (x_1, \dots, x_T)$, tokens are first mapped to embeddings $\mathbf{H}^{(0)} \in \mathbb{R}^{T \times d}$, with d being the hidden dimension. $\mathbf{H}^{(0)}$ are then processed layer by layer as $\mathbf{H}^{(l)} = F^{(l)}(\mathbf{H}^{(l-1)})$ ($1 \leq l \leq L$). For any prefix depth $L' \leq L$, we define the composite mapping $\mathbf{H}^{(L')} = F_{\leq L'}(\mathbf{H}^{(0)})$ with $F_{\leq L'} = F^{(L')} \circ \dots \circ F^{(1)}$. Due to causal attention, the last-token representation $\mathbf{h}_T^{(l)} = \mathbf{H}^{(l)}[:, T]$ summarizes the entire input at layer l (Wang et al., 2024b;d;e; Dong et al., 2025b). We therefore use $\mathbf{h}_T^{(l)}$ as latent signals and introduce L lightweight estimators

$$\phi_{\theta_l}(\mathbf{h}_T^{(l)}(\mathbf{x})) : \mathbb{R}^d \rightarrow \mathbb{R} \quad (1 \leq l \leq L) \quad (11)$$

to predict the normalized $N_{\mathbf{x}}^*/N_{\max}$. Here, normalizing $N_{\mathbf{x}}$ to $[0, 1]$ stabilizes training and prevents abnormal gradients.

We collect a batch of data with distribution P_{data} to train these estimators. For $(\mathbf{x}, \mathbf{y}) \sim P_{\text{data}}$, we first feed \mathbf{x} into π_{θ} to obtain $\mathbf{h}_T^{(l)}(\mathbf{x})$ ($1 \leq l \leq L$). We then sampling N_{\max} times to derive its $A_{\mathbf{x}}(N)$ as Eq.2 and $N_{\mathbf{x}}^*$ as Eq.3. Each estimator is trained by minimizing the expected squared loss

$$\mathcal{L}_l = \mathbb{E}_{\mathbf{x} \sim P_{\text{data}}} \left[\left(\phi_{\theta_l}(\mathbf{h}_T^{(l)}(\mathbf{x})) - \frac{N_{\mathbf{x}}^*}{N_{\max}} \right)^2 \right]. \quad (12)$$

Architecture and Training. For the estimator architecture, we follow the principle of minimal algebraic structure to employ a lightweight network: a single-hidden-layer

MLP with a ReLU activation, followed by a logistic regression output layer to adapt the regression objective. Formally,

$$\phi_{\theta_l}(\mathbf{h}) = \sigma \left(\mathbf{w}_2^\top \text{ReLU}(\mathbf{W}_1 \mathbf{h} + \mathbf{b}_1) + b_2 \right), \quad (13)$$

where $\sigma(\cdot)$ denotes the logistic sigmoid function $\frac{1}{1+e^{-\cdot}}$. We have also tested more complex architectures like deeper MLPs and shallow Transformers, but found no clear performance gains. We therefore adopt the simplest estimator that provides effective estimation with minimal cost and no overfitting. Let d be the hidden dimension of the language model, we set the hidden size of MLP as $\lfloor rd \rfloor$ with $r = 1/8$.

For the training dataset, we adopt the DeepMath-103K (He et al., 2025), which is large-scale, covers diverse mathematical domains, and spans a wide range of difficulty levels, providing sufficient diversity for feature learning and even out-of-domain generalization. Each estimator is trained on 5,000 samples and requires only about 30 seconds of training. More training details are provided in Appendix E.

Estimation Performance. We adopt Mean Absolute Error (MAE) as the evaluation metric, as it directly measures estimation accuracy and aligns with our regression objective. Results are shown in Figure 5. Since the training data are from the mathematical domain, GPQA and MMLU-Pro are treated as out-of-domain (OOD). Overall, estimators achieve high accuracy across models and datasets: MAE is around 0.1 on in-domain data and mostly below 0.2 on OOD data, indicating good generalization. Across models, Qwen and R1-Distill perform better, while Llama3.1 is relatively weaker, suggesting that estimator performance is sensitive to model representations and that cross-model generalization is challenging. Across layers, intermediate layers (gray shade area) are more stable than earlier and later layers, which often show large MAE fluctuations. This indicates that intermediate representations provide more robust features, aligning with the findings in Skean et al. (2025).

4.2. T2: Thinking Parallelism Before Parallel Thinking

Building on the above, we propose T2, an efficient parallel thinking method. As shown in Figure 2, we insert L estimators between input encoding and output decoding, and defer decoding until the optimal parallelism level is estimated.

The remaining challenge is to obtain a reliable estimate. A straightforward approach is to select the best layer based on validation performance. Specifically, we choose the layer

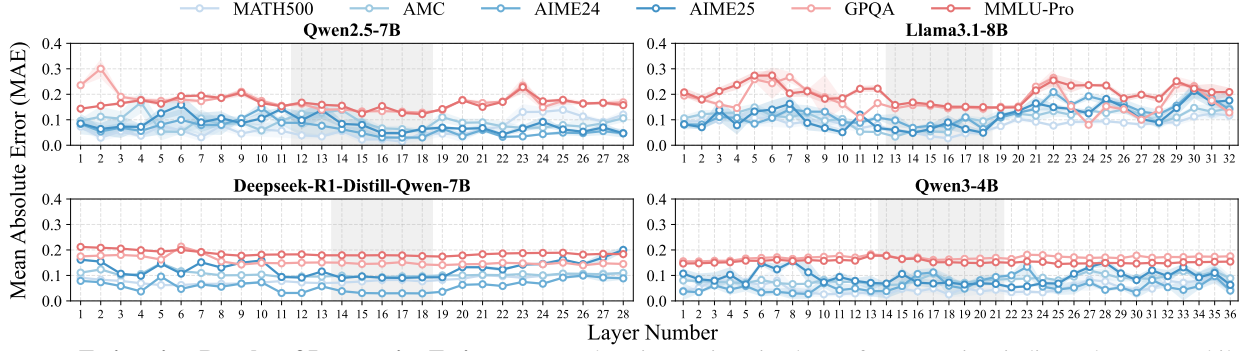


Figure 5. **Estimation Results of Layer-wise Estimators.** Each estimator is trained *over 8 runs*. Points indicate the mean, while the shaded areas indicate the standard deviation. Datasets with blue lines denote in-domain, and red lines denote out-of-domain datasets.

with the lowest validation error, denoted by L' , and compute

$$\hat{N}_{\mathbf{x}}^* = \phi_{\theta_{L'}} \left(\mathbf{h}_T^{(L')}(\mathbf{x}) \right) \cdot N_{\max}. \quad (14)$$

as the final estimate. This strategy considers system-level performance; however, Figure 5 shows that even the best-performing layer offers no significant advantage over others, leading to potential noisy decisions. Moreover, it ignores sample heterogeneity, for different layers may be optimal for different samples, leading to potential sample-level bias.

To fill this gap, we aggregate estimates from all layers through a weighted combination, allowing each layer to contribute while preserving system-level reliability. Let $\hat{n}_{\mathbf{x},l}^* = \phi_{\theta_l}(f_{\leq l}(\mathbf{x}))$ denote the estimate from layer l for input \mathbf{x} . We consider a general linear aggregation

$$\hat{N}_{\mathbf{x}}^* = N_{\max} \cdot \sum_{l=1}^L w_l \hat{n}_{\mathbf{x},l}^*, \quad \text{s.t.} \quad \sum_{l=1}^L w_l = 1, \quad (15)$$

where the weights $\mathbf{w} = (w_1, \dots, w_L)^\top$ are expected to reduce the estimation error relative to single-layer estimators.

Theorem 4.1. Fix an input \mathbf{x} . Assume each estimate $\hat{n}_{\mathbf{x},l}^*$ is unbiased, with estimation error $\varepsilon_l = \hat{n}_{\mathbf{x},l}^* - \frac{N_{\mathbf{x}}^*}{N_{\max}}$. Let $\boldsymbol{\varepsilon} = (\varepsilon_1, \dots, \varepsilon_L)^\top$ and error covariance matrix $\Sigma = \mathbb{E}[\boldsymbol{\varepsilon}\boldsymbol{\varepsilon}^\top] \succ 0$. Consider linear aggregation in Eq. 15, the weight vector

$$\mathbf{w}^* = \frac{\Sigma^{-1}\mathbf{1}}{\mathbf{1}^\top \Sigma^{-1}\mathbf{1}} \quad (16)$$

minimizes the mean squared error over all feasible \mathbf{w} , and

$$\mathbb{E} \left[\left(\sum_{l=1}^L w_l \hat{n}_{\mathbf{x},l}^* - \frac{N_{\mathbf{x}}^*}{N_{\max}} \right)^2 \right] \leq \min_{1 \leq l \leq L} \mathbb{E} \left[\left(\hat{n}_{\mathbf{x},l}^* - \frac{N_{\mathbf{x}}^*}{N_{\max}} \right)^2 \right]. \quad (17)$$

See Appendix B.3 for the proof. In theory, $\mathbf{w}^* \propto \Sigma^{-1}\mathbf{1}$, but computing the complete Σ is impractical. We therefore adopt a diagonal surrogate $\Sigma \approx \text{diag}(\sigma_1^2, \dots, \sigma_L^2)$ by ignoring error correlations, which yields inverse-variance weighting $w_l \propto 1/\sigma_l^2$. Now we can directly estimate σ_l^2 using the validation Mean Squared Error (MSE) $\hat{\sigma}_l^2$ of each layer on a validation set drawn from P_{data} (see Appendix E for details). The final weights are

$$w_l = \frac{1/\hat{\sigma}_l^2}{\sum_{i=1}^L 1/\hat{\sigma}_i^2}. \quad (18)$$

In addition, for the approximation error of the diagonal surrogate, we provide an analysis in Appendix B.4.

5. Experiments

5.1. Evaluation Setup

In this section, we evaluate how effectively our method breaks the overscaling curse, *i.e.*, how much **computational cost** it saves in practical deployment relative to the standard parallel thinking (*Std-PT*) paradigm (Section 2.1), and how this efficiency improvement affects **accuracy**. For the *Std-PT*, the parallelism level $N_{\mathcal{D}}$ is set according to Eq. 4 to maximize performance, with all $N_{\mathcal{D}}$ values shown in Figure 3. Besides, we also compare our method with several efficient methods that employ an **adaptive sampling budget** idea similar to ours, including ASC (Aggarwal et al., 2023), ESC (Li et al., 2024), DSC (Wang et al., 2025a), and DeepConf of the online version (Fu et al., 2025). Detailed descriptions of these methods are provided in Appendix F.1.

To measure computational cost, we consider both *memory overhead* and *inference latency* following Wang et al. (2025b). For memory overhead, all methods incur costs from model weights and the KV cache, with the latter being the primary contributor; our method additionally introduces estimator overhead. For each model-dataset pair, we take *Std-PT* as the reference and report the average memory cost per sample as a ratio relative to it, denoted by \mathcal{C}_{mem} . For inference latency, we measure wall-clock time including all non-decoding operations (*e.g.*, estimator inference in our method and LLM-based difficulty ranking in DSC), and report the resulting time as a ratio to *Std-PT*, denoted by $\mathcal{C}_{\text{time}}$. Detailed calculations are provided in Appendix F.2.

5.2. Main Results (Table 3)

Computational Cost. T2 consistently delivers more than 50% memory savings in most settings and ranks first or second in over 90% of cases, and is comparable to other methods. More importantly, the core strength of T2 is its inference latency, which is markedly lower than that of other methods. The key difference is that we determine the per-sample budget *before decoding*, whereas others make dynamic decisions *during decoding*, such as deciding whether to terminate or continue sampling after each sampling (AC,

Breaking the Overscaling Curse: Thinking Parallelism Before Parallel Thinking

Table 3. Computational cost (memory C_{mem} and latency C_{time} , both the ratio relative to *Std-PT*.) and accuracy (*Acc.*) across models and datasets. *Std-PT*. denotes Standard Parallel Thinking (Section 2.1), with its $N_{\mathcal{D}}$ set by Eq.4 to maximize *Acc.* **Bold** and underline denote the best and second best, respectively, among all efficient methods. **Blue** indicates higher *Acc.* than *Std-PT*., while **red** indicates higher cost than *Std-PT*. ($C_{\text{mem}} > 1$ or $C_{\text{time}} > 1$). Each result is averaged *over 32 runs*, with standard deviations in Appendix G.1.

Method	MATH500			AMC			AIME24			AIME25			GPQA			MMLU-Pro		
	$C_{\text{mem}} \downarrow$	$C_{\text{time}} \downarrow$	<i>Acc.</i> \uparrow	$C_{\text{mem}} \downarrow$	$C_{\text{time}} \downarrow$	<i>Acc.</i> \uparrow	$C_{\text{mem}} \downarrow$	$C_{\text{time}} \downarrow$	<i>Acc.</i> \uparrow	$C_{\text{mem}} \downarrow$	$C_{\text{time}} \downarrow$	<i>Acc.</i> \uparrow	$C_{\text{mem}} \downarrow$	$C_{\text{time}} \downarrow$	<i>Acc.</i> \uparrow	$C_{\text{mem}} \downarrow$	$C_{\text{time}} \downarrow$	<i>Acc.</i> \uparrow
Qwen2.5-7B																		
<i>Std-PT.</i>	1.00	1.00	79.37	1.00	1.00	49.36	1.00	1.00	16.72	1.00	1.00	10.06	1.00	1.00	39.49	1.00	1.00	60.18
AC	0.24	1.49	78.26	0.28	2.32	48.67	0.74	3.46	16.65	0.66	2.83	9.94	0.38	2.70	38.79	0.32	2.03	59.88
ESC	0.52	2.77	78.58	0.34	1.90	48.77	0.32	0.96	16.72	0.33	1.45	10.02	0.36	2.27	39.05	0.28	1.78	59.88
DSC	0.44	1.43	78.33	0.31	2.16	48.85	0.27	1.83	15.52	0.28	0.97	8.89	0.31	2.18	38.12	0.40	3.74	59.59
DeepConf	0.45	3.45	78.82	0.38	2.67	47.67	1.13	3.16	15.08	0.78	1.88	10.25	0.53	3.41	39.19	0.61	3.21	60.03
T2 (Ours)	0.18	0.48	<u>78.68</u>	0.23	0.44	49.02	0.49	0.82	17.04	<u>0.35</u>	0.68	10.32	0.27	0.51	<u>39.17</u>	0.23	0.39	60.10
Llama3.1-8B																		
<i>Std-PT.</i>	1.00	1.00	58.89	1.00	1.00	27.37	1.00	1.00	9.15	1.00	1.00	6.57	1.00	1.00	36.66	1.00	1.00	52.54
AC	0.18	1.71	57.90	0.21	2.27	26.73	0.34	3.56	8.85	0.41	3.50	<u>6.08</u>	0.37	2.99	36.24	0.31	3.17	<u>52.58</u>
ESC	0.34	1.40	58.65	0.53	2.03	26.56	0.33	1.64	9.28	0.21	2.44	5.99	0.32	2.38	<u>36.45</u>	0.35	2.16	52.63
DSC	0.28	1.75	57.38	0.33	2.18	26.56	0.27	1.63	7.78	0.14	0.98	4.35	0.26	2.08	35.92	0.26	2.83	52.00
DeepConf	0.44	2.37	58.12	0.48	2.61	26.82	0.67	4.02	7.32	0.72	5.22	4.87	0.52	4.17	34.49	0.63	4.16	49.86
T2 (Ours)	<u>0.23</u>	0.41	<u>58.46</u>	0.16	0.37	27.00	0.22	0.43	9.34	<u>0.17</u>	0.52	6.38	0.25	0.37	36.50	0.22	0.42	52.37
Deepseek-R1-Distill-Qwen-7B																		
<i>Std-PT.</i>	1.00	1.00	94.24	1.00	1.00	86.78	1.00	1.00	79.11	1.00	1.00	68.67	1.00	1.00	55.29	1.00	1.00	76.02
AC	0.28	1.89	93.70	0.32	2.77	85.82	0.44	2.50	78.64	0.37	2.75	67.79	0.54	2.62	54.67	0.47	2.32	75.72
ESC	0.15	0.84	94.02	0.27	1.72	86.03	0.53	2.19	78.39	0.41	2.19	68.12	0.43	1.67	55.42	0.38	1.92	75.37
DSC	0.45	2.13	91.04	0.39	2.89	81.28	0.56	3.58	73.75	0.32	2.00	65.30	0.60	4.03	52.99	0.35	1.79	71.14
DeepConf	0.53	3.86	93.45	0.58	3.56	85.52	0.83	4.98	79.58	0.75	3.57	68.90	0.65	3.80	53.13	0.59	3.88	73.40
T2 (Ours)	<u>0.19</u>	0.37	94.32	0.22	0.48	<u>85.97</u>	0.34	0.71	<u>79.30</u>	0.26	0.50	<u>68.28</u>	0.25	0.45	55.53	0.23	0.49	75.84
Qwen3-4B																		
<i>Std-PT.</i>	1.00	1.00	92.52	1.00	1.00	82.60	1.00	1.00	57.21	1.00	1.00	54.00	1.00	1.00	65.33	1.00	1.00	71.98
AC	0.18	1.56	92.17	0.14	2.67	81.73	0.84	3.12	56.81	0.26	2.41	53.81	0.21	2.11	65.03	0.30	2.36	71.72
ESC	0.12	0.88	<u>92.11</u>	0.23	1.84	81.77	0.55	1.93	56.34	0.28	2.25	<u>53.86</u>	0.32	1.97	<u>65.12</u>	0.34	2.23	71.90
DSC	0.16	1.35	91.17	0.28	1.71	81.32	0.72	2.21	56.18	0.22	2.78	50.23	0.36	3.92	64.21	0.39	2.97	70.38
DeepConf	0.29	2.77	91.87	0.32	3.27	81.65	1.19	4.63	57.30	0.24	3.76	52.97	0.49	3.20	64.87	0.58	4.99	<u>72.15</u>
T2 (Ours)	0.20	0.45	91.96	0.10	0.52	81.87	<u>0.57</u>	0.79	<u>57.01</u>	0.17	0.56	54.15	<u>0.27</u>	0.46	65.17	0.22	0.40	72.20

DeepConf) or batch (ESC, DSC). Therefore, they must decompose a single high-parallelism request as *Std-PT*. into a sequence of low-parallelism calls, so that undermine the concurrency of modern inference engines. In practice, we find that a single parallel request with $N = 128$ incurs only about $2 - 3 \times$ the latency of an $N = 1$ request. Consequently, serializing such requests is highly detrimental to latency, which explains why other methods often suffer increased latency despite achieving substantial memory savings. In contrast, by estimating the budget in advance, **T2 preserves full GPU parallelization throughout decoding, enabling truly efficient parallel thinking.** Notably, our estimators are lightweight, adding only tens of megabytes of memory and milliseconds of latency, which are negligible compared to the KV cache and decoding time, respectively. Detailed inference latency results are in Appendix G.2.

Performance. T2 maintains accuracy comparable to *Std-PT*. under substantial cost reductions, with any drop typically within one point. Compared with other methods, T2 always achieves the best or second-best accuracy and exceeds *Std-PT*. most frequently (8/24). Among other methods, AC and ESC exhibit relatively stable results because they rely only on the answer distribution as a model-free prior for early stopping. In contrast, DSC and DeepConf use model-based priors: DSC requires the model to rank problem difficulties, while DeepConf leverages the model’s internal con-

fidence. Although these priors provide more information, the effectiveness of such information representations across different models remains uncertain. From current results, their cross-model performances vary. For example, DeepConf performs well overall on R1-Distill-Qwen-7B but is less effective on Llama3.1-8B. In contrast, T2 leverages learnable estimators that capture richer model-specific signals. Although this satisfies a small training and inference cost, it ensures stability across models, and it also raises the performance ceiling, since if estimating perfectly, $\mathbb{E}_{(x,y) \sim P_{\mathcal{D}}} [A_x(N_x^*)] \geq \mathbb{E}_{(x,y) \sim P_{\mathcal{D}}} [A_x(N_{\mathcal{D}})]$. This is why T2 surpasses *Std-PT*. more frequently than other methods. Thus, **T2 trades a small estimator cost for greater performance potential; nevertheless, it remains more cost-efficient overall than other methods.**

In addition, **T2 also shows robust generalization on out-of-domain tasks.** Although estimators are trained on mathematical data, it performs consistently well on GPQA and MMLU-Pro, indicating robust domain generalization.

5.3. Sample Type Analysis

In Section 3.3, we categorize samples into five types to analyze the overscaling mechanism. Here, we analyze T2’s estimated optimal parallelism for each type and compare its performance with *Std-PT*. Results are shown in Table 4.

Table 4. Estimated and ground-truth optimal parallelism levels and the corresponding accuracies for each sample type in Qwen3-4B.

	MATH500					AMC					AIME24					AIME25					GPQA					MMLU-Pro				
	(1)	(2)	(3)	(4)	(5)	(1)	(2)	(3)	(4)	(5)	(1)	(2)	(3)	(4)	(5)	(1)	(2)	(3)	(4)	(5)	(1)	(2)	(3)	(4)	(5)	(1)	(2)	(3)	(4)	(5)
Optimal Parallelism Level																														
$E_{P_{(w,p,T)}} N_{\mathcal{D}}^*$ (Ground Truth)	1.0	1.0	4.3	14.6	21.2	1.0	1.0	1.3	42.1	24.1	1.0	1.0	5.5	16.2	9.9	1.0	1.0	2.7	51.7	2.0	1.0	1.0	3.3	46.7	8.2	1.0	1.0	6.1	39.9	6.7
$E_{P_{(w,p,T)}} N_{\mathcal{E}}^*$ (Estimate)	5.4	8.2	8.9	23.2	17.3	5.7	6.3	14.4	27.4	18.3	3.5	7.2	11.2	24.5	11.4	2.4	2.6	13.2	38.2	7.0	6.7	6.0	14.3	30.3	18.6	8.3	9.2	13.2	28.9	13.0
Accuracy																														
Decoding w/ $N_{\mathcal{D}}^*$ (Upper Bound)	100.00	0.00	8.38	97.23	17.63	100.00	0.00	12.23	88.07	14.00	100.00	0.00	13.23	69.02	20.04	100.00	0.00	19.22	63.45	9.30	100.00	0.00	9.23	74.08	19.29	100.00	0.00	22.54	78.02	15.33
Decoding w/ $N_{\mathcal{D}}$ (<i>Std-PT</i>)	100.00	0.00	3.54	95.14	16.38	100.00	0.00	1.78	86.28	12.03	100.00	0.00	5.84	66.62	18.30	100.00	0.00	1.49	61.41	8.52	100.00	0.00	4.43	72.12	18.23	100.00	0.00	5.99	75.93	14.32
Decoding w/ $N_{\mathcal{E}}^*$ (T2)	100.00	0.00	6.86	94.89	16.12	100.00	0.00	8.76	83.94	11.85	100.00	0.00	11.24	65.07	18.42	100.00	0.00	18.48	60.64	8.67	100.00	0.00	7.23	71.42	17.42	100.00	0.00	18.98	75.21	14.71

 Table 5. The upper panel reports the accuracy of *Std-PT* under each configuration. In the lower panel, **Tr.** and **In.** denote training and inference. Grey cells indicate ID evaluation, while the others are OOD evaluation. Results are from Qwen3-4B on AIME25.

		Acc. \uparrow											
<i>Std-PT</i> :		(a) 54.00			(b) 53.65			(c) 53.82			(d) 53.44		
Tr.	In.	$C_{\text{mem}} \downarrow$				$C_{\text{time}} \downarrow$				Acc. \uparrow			
		(a)	(b)	(c)	(d)	(a)	(b)	(c)	(d)	(a)	(b)	(c)	(d)
(a)	0.17	0.17	0.19	0.18	0.56	0.55	0.59	0.56	54.15	53.41	53.62	53.17	
(b)	0.19	0.18	0.19	0.19	0.59	0.60	0.55	0.57	53.94	53.55	53.63	53.53	
(c)	0.15	0.15	0.15	0.16	0.54	0.53	0.53	0.57	53.92	53.32	53.71	53.21	
(d)	0.21	0.23	0.21	0.23	0.61	0.59	0.61	0.62	53.78	53.34	53.45	53.50	

Despite some estimation bias, T2 largely preserves the relative order of optimal parallelism between types, with type-(4) requiring the largest budget. For type-(1) and type-(2), performance is fixed. Type-(5) also shows only minor performance variation, and its estimate bias varies across datasets. For these types, estimation mainly affects computational cost, with little impact on accuracy. In contrast, estimation quality matters more for type-(3) and type-(4). Type-(3) is slightly overestimated but remains far below $N_{\mathcal{D}}$, thus yielding gains over *Std-PT*. For type-(4), underestimation is more common and can keep the model from reaching its saturation regime, hurting accuracy. Overall, most gains for the dataset come from type-(3), and robust estimation for type-(4) is key to preserving performance. For the others, robust estimation mainly stabilizes computational cost.

5.4. Sampling Hyperparameter Adaptation

We also evaluate T2’s adaptability to sampling hyperparameters in two settings: *in-domain* (ID) and *out-of-domain* (OOD). In ID, the hyperparameters used to train the estimator are aligned with those used during model inference. In OOD, we fix the inference hyperparameters but change those used to train the estimator, creating a training-inference mismatch. We consider four sampling configurations (k, p, T) about top- k , top- p , and temperature T : (a) (20, 0.95, 0.6) (main setup), (b) (40, 0.95, 0.6), (c) (20, 0.8, 0.6), and (d) (20, 0.95, 1). Results are shown in Table 5.

In ID, cost fluctuations come mainly from hyperparameter-dependent shifts in the optimal parallelism level. As for accuracy, the gaps between T2 and the corresponding *Std-PT* are +0.15, -0.10, -0.09, and +0.06 under the four configurations, which is within a reasonable range. This suggests that **T2 adapts well and is largely insensitive to the sampling hyperparameters**. OOD is more challenging, and training-inference mismatches can cause mild performance drops. Still, the worst-case degradation is capped at 0.5,

which remains acceptable. Importantly, the drop correlates with the cost gap: larger cost discrepancies typically coincide with larger accuracy losses. Since cost is a proxy for the optimal parallelism level, a bigger mismatch implies a larger deviation from the inference-time optimum, making degradation more likely. Overall, these results show that **T2 generalizes robustly under hyperparameter shifts**.

5.5. Estimator Ablation

We also ablate the hidden-layer size and training data size of the estimator, with detailed discussion in Appendix G.3.

6. Discussion and Limitation

This work provides the first joint analysis of system-level efficacy and sample-level efficiency in parallel thinking, and uncovers an overscaling curse that creates substantial cost redundancy under system-level evaluation. Some prior studies observed that increasing the sampling budget may cause dataset performance to plateau or even degrade (Chen et al., 2024; Wen et al., 2025), but remain at an intuitive, system-level perspective without going beyond to investigate the generality and underlying mechanisms. Besides this, we link the optimal parallelism level to internal model representations, revealing latent correlations that enable input-adaptive budgets. This design trades a minimal estimator cost for significant cost savings during decoding, facilitating efficient parallel thinking. Full related work is in Appendix A.

Despite these, our work has several limitations. From the analysis perspective, we focus on stochastic sampling with majority voting, and do not cover more parallel strategies (e.g., tree search). Due to space limitations, in this work, we mainly focus on this **minimal-prior** setup to improve the reliability and scalability of our conclusions and their broader significance to the current research community. Since **our analysis framework is well defined and highly reproducible**, it can be easily extended to other strategies in future work. From the methodological perspective, we do not consider open-ended tasks, since the lack of reliable ground truth makes it difficult to define an optimal budget. In fact, evaluating open-ended results remains an open challenge, and our framework can be easily applied once suitable protocols emerge. In addition, T2 requires access to internal model states, so it currently applies only to open-source models. As the open-source community grows, we believe that this does not diminish the impact of our contribution.

Impact Statement

This paper presents work whose goal is to advance the field of machine learning. There are many potential societal consequences of our work, none of which we feel must be specifically highlighted here.

References

- Achiam, J., Adler, S., Agarwal, S., Ahmad, L., Akkaya, I., Aleman, F. L., Almeida, D., Altenschmidt, J., Altman, S., Anadkat, S., et al. Gpt-4 technical report. *arXiv preprint arXiv:2303.08774*, 2023.
- Aggarwal, P., Madaan, A., Yang, Y., et al. Let’s sample step by step: Adaptive-consistency for efficient reasoning and coding with llms. In *Proceedings of the 2023 Conference on Empirical Methods in Natural Language Processing*, pp. 12375–12396, 2023.
- Brown, B., Juravsky, J., Ehrlich, R., Clark, R., Le, Q. V., Ré, C., and Mirhoseini, A. Large language monkeys: Scaling inference compute with repeated sampling. *arXiv preprint arXiv:2407.21787*, 2024.
- Brown, T., Mann, B., Ryder, N., Subbiah, M., Kaplan, J. D., Dhariwal, P., Neelakantan, A., Shyam, P., Sastry, G., Askell, A., et al. Language models are few-shot learners. *Advances in neural information processing systems*, 33: 1877–1901, 2020.
- Chen, L., Davis, J., Hanin, B., Bailis, P., Stoica, I., Zaharia, M., and Zou, J. Are more llm calls all you need? towards the scaling properties of compound ai systems. *Advances in Neural Information Processing Systems*, 37:45767–45790, 2024.
- Chen, M., Hui, B., Cui, Z., Yang, J., Liu, D., Sun, J., Lin, J., and Liu, Z. Parallel scaling law for language models. *arXiv preprint arXiv:2505.10475*, 2025a.
- Chen, X., Xu, J., Liang, T., He, Z., Pang, J., Yu, D., Song, L., Liu, Q., Zhou, M., Zhang, Z., et al. Do not think that much for $2+3=?$ on the overthinking of long reasoning models. In *Forty-second International Conference on Machine Learning*, 2025b.
- Ding, Y., Jiang, W., Liu, S., Jing, Y., Guo, J., Wang, Y., Zhang, J., Wang, Z., Liu, Z., Du, B., et al. Dynamic parallel tree search for efficient llm reasoning. *arXiv preprint arXiv:2502.16235*, 2025.
- Dong, H., Brandfonbrener, D., Helenowski, E., He, Y., Kumar, M., Fang, H., Chi, Y., and Sankararaman, K. A. Generalized parallel scaling with interdependent generations. *arXiv preprint arXiv:2510.01143*, 2025a.
- Dong, Z., Zhou, Z., Liu, Z., Yang, C., and Lu, C. Emergent response planning in llms. *arXiv preprint arXiv:2502.06258*, 2025b.
- Fan, A., Lewis, M., and Dauphin, Y. Hierarchical neural story generation. In *Proceedings of the 56th Annual Meeting of the Association for Computational Linguistics (Volume 1: Long Papers)*, pp. 889–898, 2018.
- Fu, Y., Wang, X., Tian, Y., and Zhao, J. Deep think with confidence. *arXiv preprint arXiv:2508.15260*, 2025.
- Gandhi, K., Chakravarthy, A., Singh, A., Lile, N., and Goodman, N. D. Cognitive behaviors that enable self-improving reasoners, or, four habits of highly effective stars. *arXiv preprint arXiv:2503.01307*, 2025.
- Grattafiori, A., Dubey, A., Jauhri, A., Pandey, A., Kadian, A., Al-Dahle, A., Letman, A., Mathur, A., Schelten, A., Vaughan, A., et al. The llama 3 herd of models. *arXiv preprint arXiv:2407.21783*, 2024.
- Guan, X., Zhang, L. L., Liu, Y., Shang, N., Sun, Y., Zhu, Y., Yang, F., and Yang, M. rstar-math: Small llms can master math reasoning with self-evolved deep thinking. *arXiv preprint arXiv:2501.04519*, 2025.
- Guo, D., Yang, D., Zhang, H., Song, J., Wang, P., Zhu, Q., Xu, R., Zhang, R., Ma, S., Bi, X., et al. Deepseek-r1 incentivizes reasoning in llms through reinforcement learning. *Nature*, 645(8081):633–638, 2025.
- He, Z., Liang, T., Xu, J., Liu, Q., Chen, X., Wang, Y., Song, L., Yu, D., Liang, Z., Wang, W., et al. Deepmath-103k: A large-scale, challenging, decontaminated, and verifiable mathematical dataset for advancing reasoning. *arXiv preprint arXiv:2504.11456*, 2025.
- Hendrycks, D., Burns, C., Kadavath, S., Arora, A., Basart, S., Tang, E., Song, D., and Steinhardt, J. Measuring mathematical problem solving with the math dataset. *arXiv preprint arXiv:2103.03874*, 2021.
- Hinton, G., Vinyals, O., and Dean, J. Distilling the knowledge in a neural network. *arXiv preprint arXiv:1503.02531*, 2015.
- Holtzman, A., Buys, J., Du, L., Forbes, M., and Choi, Y. The curious case of neural text degeneration. *arXiv preprint arXiv:1904.09751*, 2019.
- Hong, C., Guo, X., Singh, A. C., Choukse, E., and Ustiugov, D. Slim-sc: Thought pruning for efficient scaling with self-consistency. In *Proceedings of the 2025 Conference on Empirical Methods in Natural Language Processing*, pp. 34488–34505, 2025.

- Jiang, D., Ren, X., and Lin, B. Y. Llm-blender: Ensembling large language models with pairwise ranking and generative fusion. In *Proceedings of the 61st Annual Meeting of the Association for Computational Linguistics (Volume 1: Long Papers)*, pp. 14165–14178, 2023.
- Kang, Z., Zhao, X., and Song, D. Scalable best-of-n selection for large language models via self-certainty. *arXiv preprint arXiv:2502.18581*, 2025.
- Li, B., Zhang, D., Wu, J., Yin, W., Tao, Z., Zhao, Y., Zhang, L., Shen, H., Fang, R., Xie, P., et al. Parallelmuse: Agentic parallel thinking for deep information seeking. *arXiv preprint arXiv:2510.24698*, 2025a.
- Li, Y., Yuan, P., Feng, S., Pan, B., Wang, X., Sun, B., Wang, H., and Li, K. Escape sky-high cost: Early-stopping self-consistency for multi-step reasoning. *arXiv preprint arXiv:2401.10480*, 2024.
- Li, Y., Gu, Q., Wen, Z., Li, Z., Xing, T., Guo, S., Zheng, T., Zhou, X., Qu, X., Zhou, W., et al. Treepo: Bridging the gap of policy optimization and efficacy and inference efficiency with heuristic tree-based modeling. *arXiv preprint arXiv:2508.17445*, 2025b.
- Liang, T., He, Z., Jiao, W., Wang, X., Wang, Y., Wang, R., Yang, Y., Shi, S., and Tu, Z. Encouraging divergent thinking in large language models through multi-agent debate. In *Proceedings of the 2024 conference on empirical methods in natural language processing*, pp. 17889–17904, 2024.
- Lightman, H., Kosaraju, V., Burda, Y., Edwards, H., Baker, B., Lee, T., Leike, J., Schulman, J., Sutskever, I., and Cobbe, K. Let’s verify step by step. In *The Twelfth International Conference on Learning Representations*, 2023.
- MAA. American mathematics competitions (amc). URL <https://maa.org/student-programs/amc/>.
- MAA. American invitational mathematics examination (aime), 2024. URL <https://maa.org/maa-invitational-competitions/>.
- MAA. American invitational mathematics examination (aime), 2025. URL <https://maa.org/maa-invitational-competitions/>.
- Muennighoff, N., Yang, Z., Shi, W., Li, X. L., Fei-Fei, L., Hajishirzi, H., Zettlemoyer, L., Liang, P., Candès, E., and Hashimoto, T. B. s1: Simple test-time scaling. In *Proceedings of the 2025 Conference on Empirical Methods in Natural Language Processing*, pp. 20286–20332, 2025.
- Ning, X., Lin, Z., Zhou, Z., Wang, Z., Yang, H., and Wang, Y. Skeleton-of-thought: Prompting llms for efficient parallel generation. *arXiv preprint arXiv:2307.15337*, 2023.
- Rein, D., Hou, B. L., Stickland, A. C., Petty, J., Pang, R. Y., Dirani, J., Michael, J., and Bowman, S. R. Gpqa: A graduate-level google-proof q&a benchmark. In *First Conference on Language Modeling*, 2024.
- Rodionov, G., Garipov, R., Shutova, A., Yakushev, G., Schultheis, E., Egiazarian, V., Sinitin, A., Kuznedelev, D., and Alistarh, D. Hogwild! inference: Parallel llm generation via concurrent attention. *arXiv preprint arXiv:2504.06261*, 2025.
- Shao, Z., Wang, P., Zhu, Q., Xu, R., Song, J., Bi, X., Zhang, H., Zhang, M., Li, Y., Wu, Y., et al. Deepseekmath: Pushing the limits of mathematical reasoning in open language models. *arXiv preprint arXiv:2402.03300*, 2024.
- Skean, O., Arefin, M. R., Zhao, D., Patel, N., Naghiyev, J., LeCun, Y., and Shwartz-Ziv, R. Layer by layer: Uncovering hidden representations in language models. *arXiv preprint arXiv:2502.02013*, 2025.
- Snell, C., Lee, J., Xu, K., and Kumar, A. Scaling llm test-time compute optimally can be more effective than scaling model parameters. *arXiv preprint arXiv:2408.03314*, 2024.
- Sun, H., Haider, M., Zhang, R., Yang, H., Qiu, J., Yin, M., Wang, M., Bartlett, P., and Zanette, A. Fast best-of-n decoding via speculative rejection. *Advances in Neural Information Processing Systems*, 37:32630–32652, 2024.
- Team, G., Anil, R., Borgeaud, S., Alayrac, J.-B., Yu, J., Soricut, R., Schalkwyk, J., Dai, A. M., Hauth, A., Millican, K., et al. Gemini: a family of highly capable multimodal models. *arXiv preprint arXiv:2312.11805*, 2023.
- Vaswani, A. Attention is all you need. *Advances in Neural Information Processing Systems*, 2017.
- Wang, H., Xiong, W., Xie, T., Zhao, H., and Zhang, T. Interpretable preferences via multi-objective reward modeling and mixture-of-experts. *arXiv preprint arXiv:2406.12845*, 2024a.
- Wang, L., Yang, N., Huang, X., Yang, L., Majumder, R., and Wei, F. Improving text embeddings with large language models. In *Proceedings of the 62nd Annual Meeting of the Association for Computational Linguistics (Volume 1: Long Papers)*, pp. 11897–11916, 2024b.
- Wang, X., Wei, J., Schuurmans, D., Le, Q., Chi, E., Narang, S., Chowdhery, A., and Zhou, D. Self-consistency improves chain of thought reasoning in language models. *arXiv preprint arXiv:2203.11171*, 2022.

- Wang, X., Feng, S., Li, Y., Yuan, P., Zhang, Y., Tan, C., Pan, B., Hu, Y., and Li, K. Make every penny count: Difficulty-adaptive self-consistency for cost-efficient reasoning. In *Findings of the Association for Computational Linguistics: NAACL 2025*, pp. 6904–6917, 2025a.
- Wang, Y., Ma, X., Zhang, G., Ni, Y., Chandra, A., Guo, S., Ren, W., Arulraj, A., He, X., Jiang, Z., et al. Mmlu-pro: A more robust and challenging multi-task language understanding benchmark. *Advances in Neural Information Processing Systems*, 37:95266–95290, 2024c.
- Wang, Y., Zhang, P., Yang, B., Wong, D., Zhang, Z., and Wang, R. Embedding trajectory for out-of-distribution detection in mathematical reasoning. *Advances in Neural Information Processing Systems*, 37:42965–42999, 2024d.
- Wang, Y., Zhang, P., Yang, B., Wong, D. F., and Wang, R. Latent space chain-of-embedding enables output-free llm self-evaluation. *arXiv preprint arXiv:2410.13640*, 2024e.
- Wang, Y., Zhang, P., Huang, S., Yang, B., Zhang, Z., Huang, F., and Wang, R. Sampling-efficient test-time scaling: Self-estimating the best-of-n sampling in early decoding. *arXiv preprint arXiv:2503.01422*, 2025b.
- Wang, Y., Zhang, P., Tang, J., Wei, H., Yang, B., Wang, R., Sun, C., Sun, F., Zhang, J., Wu, J., et al. Polymath: Evaluating mathematical reasoning in multilingual contexts. *arXiv preprint arXiv:2504.18428*, 2025c.
- Wen, H., Su, Y., Zhang, F., Liu, Y., Liu, Y., Zhang, Y.-Q., and Li, Y. Parathinker: Native parallel thinking as a new paradigm to scale llm test-time compute. *arXiv preprint arXiv:2509.04475*, 2025.
- Wiseman, S. and Rush, A. M. Sequence-to-sequence learning as beam-search optimization. *arXiv preprint arXiv:1606.02960*, 2016.
- Wu, T., Liu, Y., Bai, J., Jia, Z., Zhang, S., Lin, Z., Wang, Y., Zhu, S.-C., and Zheng, Z. Native parallel reasoner: Reasoning in parallelism via self-distilled reinforcement learning. *arXiv preprint arXiv:2512.07461*, 2025.
- Xiong, M., Hu, Z., Lu, X., Li, Y., Fu, J., He, J., and Hooi, B. Can llms express their uncertainty? an empirical evaluation of confidence elicitation in llms. *arXiv preprint arXiv:2306.13063*, 2023.
- Yang, A., Yang, B., Zhang, B., Hui, B., Zheng, B., Yu, B., Li, C., Liu, D., Huang, F., Wei, H., et al. Qwen2.5 technical report. *arXiv preprint arXiv:2412.15115*, 2024.
- Yang, A., Li, A., Yang, B., Zhang, B., Hui, B., Zheng, B., Yu, B., Gao, C., Huang, C., Lv, C., et al. Qwen3 technical report. *arXiv preprint arXiv:2505.09388*, 2025a.
- Yang, X., An, Y., Liu, H., Chen, T., and Chen, B. Multiverse: Your language models secretly decide how to parallelize and merge generation. *arXiv preprint arXiv:2506.09991*, 2025b.
- Yao, S., Yu, D., Zhao, J., Shafran, I., Griffiths, T., Cao, Y., and Narasimhan, K. Tree of thoughts: Deliberate problem solving with large language models. *Advances in neural information processing systems*, 36:11809–11822, 2023.
- Ye, Y., Huang, Z., Xiao, Y., Chern, E., Xia, S., and Liu, P. Limo: Less is more for reasoning. *arXiv preprint arXiv:2502.03387*, 2025.
- Yu, Q., Zhang, Z., Zhu, R., Yuan, Y., Zuo, X., Yue, Y., Dai, W., Fan, T., Liu, G., Liu, L., et al. Dapo: An open-source llm reinforcement learning system at scale. *arXiv preprint arXiv:2503.14476*, 2025.
- Zeng, W., He, K., Kuang, C., Li, X., and He, J. Pushing test-time scaling limits of deep search with asymmetric verification. *arXiv preprint arXiv:2510.06135*, 2025.
- Zhang, D., Huang, X., Zhou, D., Li, Y., and Ouyang, W. Accessing gpt-4 level mathematical olympiad solutions via monte carlo tree self-refine with llama-3 8b. *arXiv preprint arXiv:2406.07394*, 2024.
- Zheng, T., Zhang, H., Yu, W., Wang, X., Dai, R., Liu, R., Bao, H., Huang, C., Huang, H., and Yu, D. Parallel-rl: Towards parallel thinking via reinforcement learning. *arXiv preprint arXiv:2509.07980*, 2025.

A. Related Work

A.1. Parallel Thinking

Parallel thinking is a test-time scaling paradigm that mainly consists of two stages: *exploratory sampling* and *answer generation* (Li et al., 2025a). In the first stage, the most brute-force strategy is stochastic methods, where each reasoning path is independently explored from scratch via multinomial sampling (Wang et al., 2022; Lightman et al., 2023; Brown et al., 2024; Chen et al., 2024; Kang et al., 2025; Wang et al., 2025b), including variants that partially relax the independence across paths (Rodionov et al., 2025; Dong et al., 2025a). Beyond this, heuristic methods provide finer-grained control during decoding. For example, Beam Search (Wiseman & Rush, 2016) increases the effective lookahead by maintaining multiple hypotheses at each decoding step. Other strategies, such as Tree-of-Thought (ToT) (Yao et al., 2023), Skeleton-of-Thought (SoT) (Ning et al., 2023), and Monte Carlo Tree Search (MCTS) (Zhang et al., 2024; Guan et al., 2025; Li et al., 2025b; Ding et al., 2025), build on stochastic rollouts or structured expansions, and introduce additional hyperparameters to regulate branching, merging, truncation, and back-propagation of sampling paths. In the second stage, majority voting is the most commonly used and minimally biased unsupervised approach, with strong generality and simplicity (Wang et al., 2022; Xiong et al., 2023; Team et al., 2023; Liang et al., 2024). Beyond this, some methods incorporate prior information into the aggregation process, such as confidence and certainty (Kang et al., 2025; Fu et al., 2025), or even introduce external priors by scoring candidates with external reward models (Aggarwal et al., 2023; Wang et al., 2024a) or LLMs (Jiang et al., 2023; Xiong et al., 2023). In this work, we adopt the simplest stochastic sampling strategy without introducing any heuristic methods, consistent with prior work (Wang et al., 2022; Chen et al., 2024; Snell et al., 2024; Brown et al., 2024; Fu et al., 2025), and involving minimal hyperparameters. Meanwhile, the aggregation strategy also adopts majority voting with minimal prior information, offering strong scalability of our conclusions. More strategies are left for our future exploration.

Another line of work has recently investigated training-based methods for further unlocking parallel thinking capabilities in LLMs, including SFT (Wen et al., 2025; Yang et al., 2025b), RL (Zheng et al., 2025; Wu et al., 2025), and architectural parallelism (Chen et al., 2025a). Since our focus is on training-free methods, these studies are totally orthogonal to our work. Overall, parallel thinking provides a promising avenue for unlocking the latent capabilities of LLMs.

A.2. Efficient Parallel Thinking

Efficient parallel thinking mainly follows two research directions (Wang et al., 2025b): *breadth pruning* and *depth pruning*. Breadth pruning adaptively allocates the sampling budget per sample, and our T2 belongs to this line. Prior methods, including AC (Aggarwal et al., 2023), ESC (Li et al., 2024), and DSC (Wang et al., 2025a), rely on answer frequency or problem difficulty for dynamic early stopping, but our experiments show that they incur substantial latency. Depth pruning keeps the overall budget fixed while shortening individual reasoning paths. For example, SBoN (Sun et al., 2024) uses a reward model to score early partial sequences and discard low-scoring paths, ST-BoN (Wang et al., 2025b) truncates unpromising samples based on internal consistency estimates, and Slim-SC (Hong et al., 2025) prunes highly similar paths on the fly during decoding. These two research lines are orthogonal, and **our T2 belongs to breadth pruning, as its efficiency gains lie in adaptive budget allocation.**

Of course, these two can also be combined. Although they are orthogonal, they are not conflicting. For example, DeepConf (Fu et al., 2025) performs path truncation on each sampling path during adaptive early stopping. Our T2 can also be seamlessly integrated with other depth-pruning methods, as it only requires estimating the optimal parallelism level before decoding. With this estimate in place, path-level pruning can still be applied during decoding without interference.

A.3. Test-time Scaling

Test-time scaling (Snell et al., 2024) aims to enhance reasoning performance by increasing computation at inference time. This paradigm follows two main research directions (Muennighoff et al., 2025): *sequential scaling* and *parallel scaling*. Sequential scaling focuses on extending the length of a single chain-of-thought to induce slower, more deliberate thinking, thereby eliciting cognitive mechanisms such as reflection and backtracking (Guo et al., 2025; Gandhi et al., 2025) that increase the likelihood of reaching the correct answer, through RL (Shao et al., 2024; Guo et al., 2025; Yu et al., 2025), SFT (Muennighoff et al., 2025; Ye et al., 2025; Yang et al., 2025a), or inference-time prompt forcing (Muennighoff et al., 2025; Wang et al., 2025c). Parallel scaling corresponds to parallel thinking, which is discussed in detail in Appendix A.1. These two paradigms are complementary and together provide a solid foundation for eliciting models’ deep reasoning capabilities.

B. Mathematical Proof and Analysis

B.1. Answer-Distribution View of the Five Sample Types in Table 1

Fix an input \mathbf{x} and a sampling configuration (e.g., top- k /top- p /temperature). Let $\mathcal{A} = \{a_1, \dots, a_m\}$ be the finite set of *canonicalized final answers* under the evaluation protocol, and let $a^* \in \mathcal{A}$ be the ground-truth answer. A single stochastic decode induces a categorical distribution

$$\mathbf{p}(\mathbf{x}) := (p_1, \dots, p_m), \quad p_j := \Pr(\text{one sample yields } a_j \mid \mathbf{x}), \quad \sum_{j=1}^m p_j = 1. \quad (19)$$

(All quantities below depend on the model and sampling hyperparameters through $\mathbf{p}(\mathbf{x})$.)

Given N i.i.d. samples $Y_1, \dots, Y_N \sim \mathbf{p}(\mathbf{x})$, let $C_j := \sum_{i=1}^N \mathbf{1}\{Y_i = a_j\}$ be the count of a_j . Majority voting (mode) outputs

$$\text{MV}_N(Y_{1:N}) \in \arg \max_{j \in [m]} C_j, \quad (20)$$

with any fixed tie-breaking rule, and the per-sample accuracy curve is

$$A_{\mathbf{x}}(N) := \Pr(\text{MV}_N(Y_{1:N}) = a^*). \quad (21)$$

To connect $A_{\mathbf{x}}(N)$ with the answer distribution, let j^* be the index of a^* , define the strongest competitor

$$\tilde{p} := \max_{j \neq j^*} p_j, \quad (22)$$

and the *margin*

$$\Delta := p_{j^*} - \tilde{p}. \quad (23)$$

Also define the top-two gap

$$p_{(1)} := \max_j p_j, \quad p_{(2)} := \max_{j \neq j_{(1)}} p_j, \quad \gamma := p_{(1)} - p_{(2)}, \quad (24)$$

where $j_{(1)} \in \arg \max_j p_j$ is any top-1 index.

If the population mode is unique (i.e., $\gamma > 0$), then standard concentration arguments imply that majority voting recovers the mode with probability approaching 1 as $N \rightarrow \infty$. Consequently,

$$A_{\mathbf{x}}(N) \rightarrow \mathbf{1}\{j^* = j_{(1)}\} \quad \text{as } N \rightarrow \infty, \quad (25)$$

namely, $A_{\mathbf{x}}(N) \rightarrow 1$ when the correct answer is the unique mode, and $A_{\mathbf{x}}(N) \rightarrow 0$ otherwise. Moreover, when $\Delta > 0$, a simple union bound yields

$$A_{\mathbf{x}}(N) \geq 1 - (m-1) \exp\left(-\frac{N}{2} \Delta^2\right), \quad (26)$$

showing that the convergence under majority voting accelerates with larger margins.

With these quantities, the five sample types in Table 1 admit a direct distributional interpretation:

- **Type-(1) (\mathcal{D}_1):** $p_{j^*} = 1$ (a point mass at the correct answer), hence $A_{\mathbf{x}}(N) \equiv 1$.
- **Type-(2) (\mathcal{D}_2):** $p_{j^*} = 0$ (the correct answer never appears), hence $A_{\mathbf{x}}(N) \equiv 0$.
- **Type-(3) (\mathcal{D}_3):** $0 < p_{j^*} < 1$ and $\Delta < 0$ (an incorrect answer is the unique mode), so $A_{\mathbf{x}}(N) \rightarrow 0$ as $N \rightarrow \infty$.
- **Type-(4) (\mathcal{D}_4):** $0 < p_{j^*} < 1$ and $\Delta > 0$ (the correct answer is the unique mode), so $A_{\mathbf{x}}(N) \rightarrow 1$ as $N \rightarrow \infty$, with faster convergence for larger Δ .
- **Type-(5) (\mathcal{D}_5):** a *finite- N regime* induced by a small top-two gap γ . For a practical budget range $N \leq N_{\max}$, when $0 < \gamma \leq \epsilon$ for small ϵ , majority voting can be sensitive to finite-sample fluctuations, and $A_{\mathbf{x}}(N)$ may exhibit no clear monotonic trend. When the mode is unique ($\gamma > 0$), this behavior eventually reduces to Type-(3) or Type-(4) as $N \rightarrow \infty$ depending on whether the unique mode is incorrect or correct, respectively; the only non-reducing case is an exact mode tie ($\gamma = 0$), where the limit depends on tie-breaking.

B.2. Proof of Theorem 3.4

Proof. We first examine the gain properties of the five sample types. Let $N^* := N_{\mathcal{D}_4}^*$. By definition, $N_{\mathcal{D}}$ is the *smallest* maximizer of $A_{\mathcal{D}}(N)$ over $N \in [1, N_{\max}]$. Hence for any $N \in [1, N_{\max}]$,

$$A_{\mathcal{D}}(N_{\mathcal{D}}) \geq A_{\mathcal{D}}(N). \quad (27)$$

In particular, taking $N = N^*$ gives

$$A_{\mathcal{D}}(N^*) - A_{\mathcal{D}}(N_{\mathcal{D}}) \leq 0. \quad (28)$$

For any $N_1 < N_2$, applying the law of total expectation yields the type-wise decomposition

$$A_{\mathcal{D}}(N_2) - A_{\mathcal{D}}(N_1) = \sum_{i=1}^5 p_i (A_{\mathcal{D}_i}(N_2) - A_{\mathcal{D}_i}(N_1)) = \sum_{i=1}^5 p_i \Delta_{\mathcal{D}_i}(N_1, N_2). \quad (29)$$

Applying (29) to $(N_1, N_2) = (N_{\mathcal{D}}, N^*)$ and combining with (28) gives

$$\sum_{i=1}^5 p_i \Delta_{\mathcal{D}_i}(N_{\mathcal{D}}, N^*) \leq 0. \quad (30)$$

At this point, we invoke the sign structure induced by the five-type construction on the interval $[1, N^*]$. In particular, for type-(1) and type-(2), the interval gain is identically zero:

$$\Delta_{\mathcal{D}_1}(N, N^*) = 0, \quad \Delta_{\mathcal{D}_2}(N, N^*) = 0, \quad \forall N \leq N^*. \quad (31)$$

Moreover, for type-(5), extending the budget does not yield positive net gain; in our simplified model we treat it as zero:

$$\Delta_{\mathcal{D}_5}(N, N^*) = 0, \quad \forall N \leq N^*. \quad (32)$$

Substituting (31)–(32) into (30) eliminates the $i \in \{1, 2, 5\}$ terms and yields

$$p_3 \Delta_{\mathcal{D}_3}(N_{\mathcal{D}}, N^*) + p_4 \Delta_{\mathcal{D}_4}(N_{\mathcal{D}}, N^*) \leq 0. \quad (33)$$

Rearranging (33) gives the two-type inequality

$$p_4 \Delta_{\mathcal{D}_4}(N_{\mathcal{D}}, N^*) \leq p_3 (-\Delta_{\mathcal{D}_3}(N_{\mathcal{D}}, N^*)). \quad (34)$$

We now connect the type-(4) gain and type-(3) loss through the definition of δ . Recall

$$\delta := \inf_{1 \leq N \leq N^*} \frac{\Delta_{\mathcal{D}_4}(N, N^*)}{-\Delta_{\mathcal{D}_3}(N, N^*)}. \quad (35)$$

Assume $N_{\mathcal{D}} < N^*$ for the moment. Then $N = N_{\mathcal{D}}$ is admissible in the infimum above, hence, by the definition of infimum,

$$\frac{\Delta_{\mathcal{D}_4}(N_{\mathcal{D}}, N^*)}{-\Delta_{\mathcal{D}_3}(N_{\mathcal{D}}, N^*)} \geq \delta. \quad (36)$$

Since $-\Delta_{\mathcal{D}_3}(N_{\mathcal{D}}, N^*) \geq 0$ under the type-(3) sign structure on $[1, N^*]$, multiplying both sides of (36) by $-\Delta_{\mathcal{D}_3}(N_{\mathcal{D}}, N^*)$ yields

$$\Delta_{\mathcal{D}_4}(N_{\mathcal{D}}, N^*) \geq \delta \cdot (-\Delta_{\mathcal{D}_3}(N_{\mathcal{D}}, N^*)). \quad (37)$$

Equivalently, dividing both sides of (37) by $\delta > 0$ gives

$$-\Delta_{\mathcal{D}_3}(N_{\mathcal{D}}, N^*) \leq \frac{1}{\delta} \Delta_{\mathcal{D}_4}(N_{\mathcal{D}}, N^*). \quad (38)$$

We now plug (38) into the two-type inequality (34). From (34) and (38), we obtain the explicit chain

$$p_4 \Delta_{\mathcal{D}_4}(N_{\mathcal{D}}, N^*) \leq p_3 \cdot \frac{1}{\delta} \Delta_{\mathcal{D}_4}(N_{\mathcal{D}}, N^*). \quad (39)$$

Rearranging (39) yields

$$\left(p_4 - \frac{p_3}{\delta}\right) \Delta_{\mathcal{D}_4}(N_{\mathcal{D}}, N^*) \leq 0, \quad (N_{\mathcal{D}} < N^*). \quad (40)$$

We now distinguish two regimes according to the value of $p_4 \delta$.

Case 1: $p_4\delta \leq 1 - p_4$. In this regime the gating condition is inactive, and the desired lower bound reduces to $N_{\mathcal{D}} \geq 1$, which holds by definition.

Case 2: $p_4\delta > 1 - p_4$. We show that this condition forces $N_{\mathcal{D}} \geq N^*$.

Since $p_1 + \dots + p_5 = 1$ and $p_i \geq 0$ for all i , we have

$$p_3 \leq 1 - p_4. \quad (41)$$

Therefore, under $p_4\delta > 1 - p_4$ we also have $p_4\delta > p_3$, which implies

$$p_4 - \frac{p_3}{\delta} > 0. \quad (42)$$

Applying (40) and using (42), we deduce

$$\Delta_{\mathcal{D}_4}(N_{\mathcal{D}}, N^*) \leq 0. \quad (43)$$

Suppose, for contradiction, that $N_{\mathcal{D}} < N^*$. By the defining property of the sample-optimal parallelism level for type-(4), extending the budget strictly improves accuracy until N^* is reached. In particular, for any $N < N^*$,

$$\Delta_{\mathcal{D}_4}(N, N^*) > 0. \quad (44)$$

Applying (44) at $N = N_{\mathcal{D}}$ yields

$$\Delta_{\mathcal{D}_4}(N_{\mathcal{D}}, N^*) > 0, \quad (45)$$

which contradicts (43). Therefore, the assumption $N_{\mathcal{D}} < N^*$ is false, and we conclude that

$$N_{\mathcal{D}} \geq N^*. \quad (46)$$

Combining the two cases above, we obtain the unified lower bound

$$N_{\mathcal{D}} \geq 1 + (N^* - 1)\mathbf{1}\{p_4\delta > 1 - p_4\}. \quad (47)$$

Finally, by definition,

$$\mathcal{M}_{\mathcal{D}} = \frac{\sum_{i=1}^5 p_i N_{\mathcal{D}_i}^*}{N_{\mathcal{D}}}. \quad (48)$$

Using $N_{\mathcal{D}_1}^* = N_{\mathcal{D}_2}^* = 1$, we can write

$$\sum_{i=1}^5 p_i N_{\mathcal{D}_i}^* = 1 + p_3(N_{\mathcal{D}_3}^* - 1) + p_5(N_{\mathcal{D}_5}^* - 1) + p_4(N^* - 1). \quad (49)$$

By definition $\kappa := N_{\mathcal{D}_3}^* + N_{\mathcal{D}_5}^* - 1$ and using $p_3 + p_5 \leq 1 - p_4$, we obtain

$$\sum_{i=1}^5 p_i N_{\mathcal{D}_i}^* \leq \kappa + p_4(N^* - \kappa). \quad (50)$$

Combining (50) with the lower bound (47), we conclude that

$$\mathcal{M}_{\mathcal{D}} \leq \frac{\kappa + p_4(N^* - \kappa)}{1 + (N^* - 1)\mathbf{1}\{p_4\delta > 1 - p_4\}} = \varphi(p_4), \quad (51)$$

which completes the proof. □

B.3. Proof of Theorem 4.1

Fix an input \mathbf{x} . For each layer $l \in \{1, \dots, L\}$, define the estimation error

$$\varepsilon_l := \hat{n}_{\mathbf{x},l}^* - \frac{N_{\mathbf{x}}^*}{N_{\max}}, \quad \boldsymbol{\varepsilon} = (\varepsilon_1, \dots, \varepsilon_L)^\top. \quad (52)$$

By the unbiasedness assumption, $\mathbb{E}[\boldsymbol{\varepsilon}] = \mathbf{0}$. Let the error covariance be $\Sigma = \mathbb{E}[\boldsymbol{\varepsilon}\boldsymbol{\varepsilon}^\top] \succ 0$.

For any weight vector $\mathbf{w} \in \mathbb{R}^L$ satisfying $\mathbf{1}^\top \mathbf{w} = 1$, define the aggregated estimator

$$\hat{n}_{\mathbf{x}}^*(\mathbf{w}) := \sum_{l=1}^L w_l \hat{n}_{\mathbf{x},l}^*. \quad (53)$$

Then

$$\hat{n}_{\mathbf{x}}^*(\mathbf{w}) - \frac{N_{\mathbf{x}}^*}{N_{\max}} = \sum_{l=1}^L w_l \varepsilon_l = \mathbf{w}^\top \boldsymbol{\varepsilon}. \quad (54)$$

Taking expectation yields

$$\mathbb{E}\left[\hat{n}_{\mathbf{x}}^*(\mathbf{w}) - \frac{N_{\mathbf{x}}^*}{N_{\max}}\right] = \mathbf{w}^\top \mathbb{E}[\boldsymbol{\varepsilon}] = 0, \quad (55)$$

so the mean squared error equals the variance:

$$\mathbb{E}\left[\left(\hat{n}_{\mathbf{x}}^*(\mathbf{w}) - \frac{N_{\mathbf{x}}^*}{N_{\max}}\right)^2\right] = \mathbb{E}[(\mathbf{w}^\top \boldsymbol{\varepsilon})^2] = \mathbf{w}^\top \mathbb{E}[\boldsymbol{\varepsilon}\boldsymbol{\varepsilon}^\top] \mathbf{w} = \mathbf{w}^\top \Sigma \mathbf{w}. \quad (56)$$

Therefore, minimizing the MSE over all linear aggregations with $\mathbf{1}^\top \mathbf{w} = 1$ is equivalent to the constrained quadratic problem

$$\min_{\mathbf{w} \in \mathbb{R}^L} \mathbf{w}^\top \Sigma \mathbf{w} \quad \text{s.t.} \quad \mathbf{1}^\top \mathbf{w} = 1. \quad (57)$$

Since $\Sigma \succ 0$, the objective is strictly convex and the feasible set is affine, so (57) admits a unique global minimizer.

Consider the Lagrangian

$$\mathcal{L}(\mathbf{w}, \lambda) = \mathbf{w}^\top \Sigma \mathbf{w} + \lambda(\mathbf{1}^\top \mathbf{w} - 1). \quad (58)$$

The first-order optimality condition gives

$$\nabla_{\mathbf{w}} \mathcal{L}(\mathbf{w}, \lambda) = 2\Sigma \mathbf{w} + \lambda \mathbf{1} = \mathbf{0}, \quad (59)$$

which implies

$$\mathbf{w} = -(\lambda/2)\Sigma^{-1}\mathbf{1}. \quad (60)$$

Enforcing $\mathbf{1}^\top \mathbf{w} = 1$ yields

$$1 = \mathbf{1}^\top \mathbf{w} = -\frac{\lambda}{2} \mathbf{1}^\top \Sigma^{-1} \mathbf{1} \implies \lambda = -\frac{2}{\mathbf{1}^\top \Sigma^{-1} \mathbf{1}}. \quad (61)$$

Substituting back gives the unique minimizer

$$\mathbf{w}^* = \frac{\Sigma^{-1} \mathbf{1}}{\mathbf{1}^\top \Sigma^{-1} \mathbf{1}}, \quad (62)$$

which is exactly Eq. (16).

Finally, let \mathbf{e}_l be the l -th standard basis vector in \mathbb{R}^L . Choosing $\mathbf{w} = \mathbf{e}_l$ corresponds to using the single-layer estimator $\hat{n}_{\mathbf{x},l}^*$. By (56),

$$\mathbb{E}\left[\left(\hat{n}_{\mathbf{x},l}^* - \frac{N_{\mathbf{x}}^*}{N_{\max}}\right)^2\right] = \mathbf{e}_l^\top \Sigma \mathbf{e}_l = \Sigma_{ll} = \mathbb{E}[\varepsilon_l^2]. \quad (63)$$

Since \mathbf{w}^* is the global minimizer of (57), we have $\mathbf{w}^{*\top} \Sigma \mathbf{w}^* \leq \mathbf{e}_l^\top \Sigma \mathbf{e}_l$ for all l , hence

$$\mathbb{E}\left[\left(\sum_{i=1}^L w_i^* \hat{n}_{\mathbf{x},i}^* - \frac{N_{\mathbf{x}}^*}{N_{\max}}\right)^2\right] \leq \mathbb{E}\left[\left(\hat{n}_{\mathbf{x},l}^* - \frac{N_{\mathbf{x}}^*}{N_{\max}}\right)^2\right], \quad \forall l \in \{1, \dots, L\}. \quad (64)$$

Taking the minimum over l gives (17), completing the proof. \square

B.4. Approximation Error of Diagonal Covariance Surrogate

▷ [Back to Section 4.2](#)

In this section, we analyze the approximation error induced by replacing the full error covariance matrix Σ with its diagonal surrogate.

Let $\varepsilon = (\varepsilon_1, \dots, \varepsilon_L)^\top$ denote the layer-wise estimation errors and $\Sigma = \mathbb{E}[\varepsilon\varepsilon^\top]$ their covariance matrix. We decompose Σ as

$$\Sigma = D + R, \quad (65)$$

where $D = \text{diag}(\Sigma)$ contains the diagonal elements and $R = \Sigma - D$ contains only the off-diagonal terms.

For any aggregation weight \mathbf{w} satisfying $\mathbf{1}^\top \mathbf{w} = 1$ and $w_l \geq 0$, the resulting mean squared error can be written as

$$\mathbf{w}^\top \Sigma \mathbf{w} = \mathbf{w}^\top D \mathbf{w} + \mathbf{w}^\top R \mathbf{w}. \quad (66)$$

The second term quantifies the approximation error introduced by ignoring cross-layer correlations. By Hölder's inequality, we have

$$|\mathbf{w}^\top R \mathbf{w}| \leq \|R\|_\infty := \max_i \sum_j |R_{ij}|, \quad (67)$$

which yields the bound

$$\mathbf{w}^\top \Sigma \mathbf{w} \in \left[\mathbf{w}^\top D \mathbf{w} - \|R\|_\infty, \mathbf{w}^\top D \mathbf{w} + \|R\|_\infty \right]. \quad (68)$$

Therefore, the worst-case deviation of the diagonal surrogate from the true aggregation error is upper bounded by $\|R\|_\infty$. In practice, we estimate the empirical covariance matrix $\hat{\Sigma}$ on the validation set and report the relative off-diagonal energy

$$\frac{\|\hat{R}\|_F}{\|\hat{\Sigma}\|_F}, \quad \hat{R} = \hat{\Sigma} - \text{diag}(\hat{\Sigma}), \quad (69)$$

as well as the relative MSE deviation

$$\frac{|\mathbf{w}^\top \hat{R} \mathbf{w}|}{\mathbf{w}^\top \hat{D} \mathbf{w}}. \quad (70)$$

Empirically, both quantities are consistently small, indicating that cross-layer error correlations contribute marginally to the aggregated MSE, and validating the diagonal approximation adopted in our method.

C. Overscaling Curse of Parallel Thinking

C.1. More Examples of Sample Types

▷ **Back to Figure 1**

- **Figure 6 - 8:** Qwen2.5-7B on MATH500
- **Figure 9 - 10:** Qwen2.5-7B on AIME2024
- **Figure 11 - 12:** Qwen2.5-7B on AIME2025
- **Figure 13 - 14:** Qwen3-4B on AIME2024
- **Figure 15 - 17:** Qwen3-4B on AIME2025

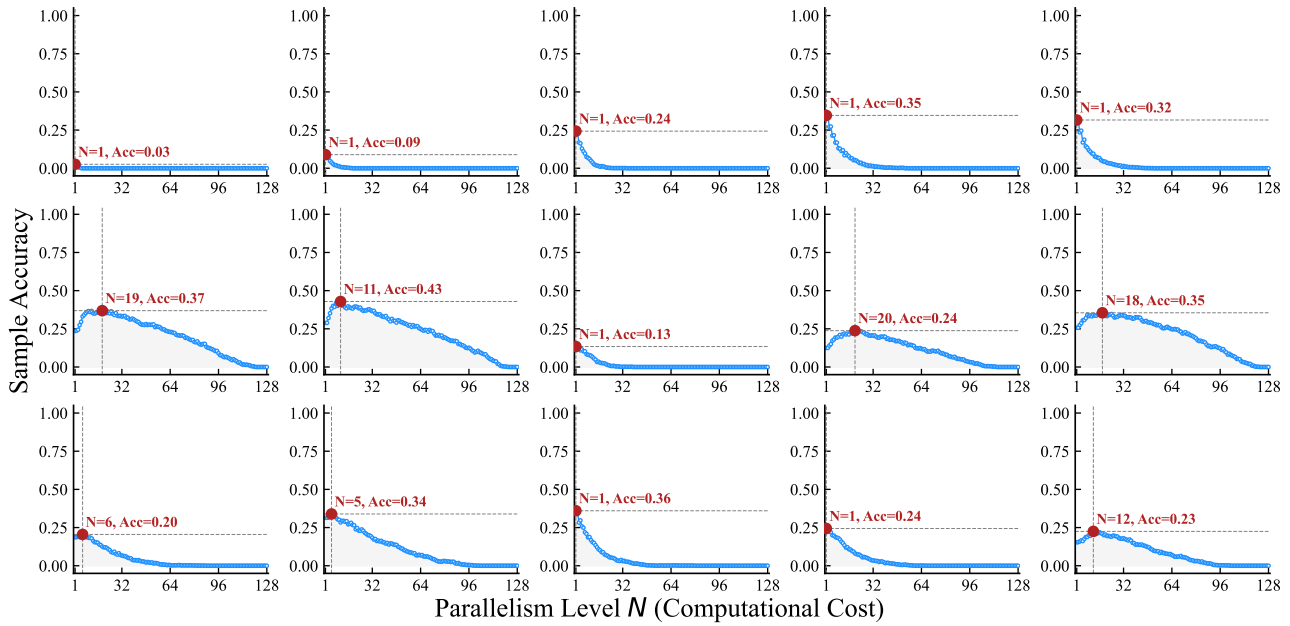


Figure 6. Examples of the “cost-accuracy” function $A_x(N)$ for **Type-(3)** samples from Qwen2.5-7B on the MATH500 dataset.

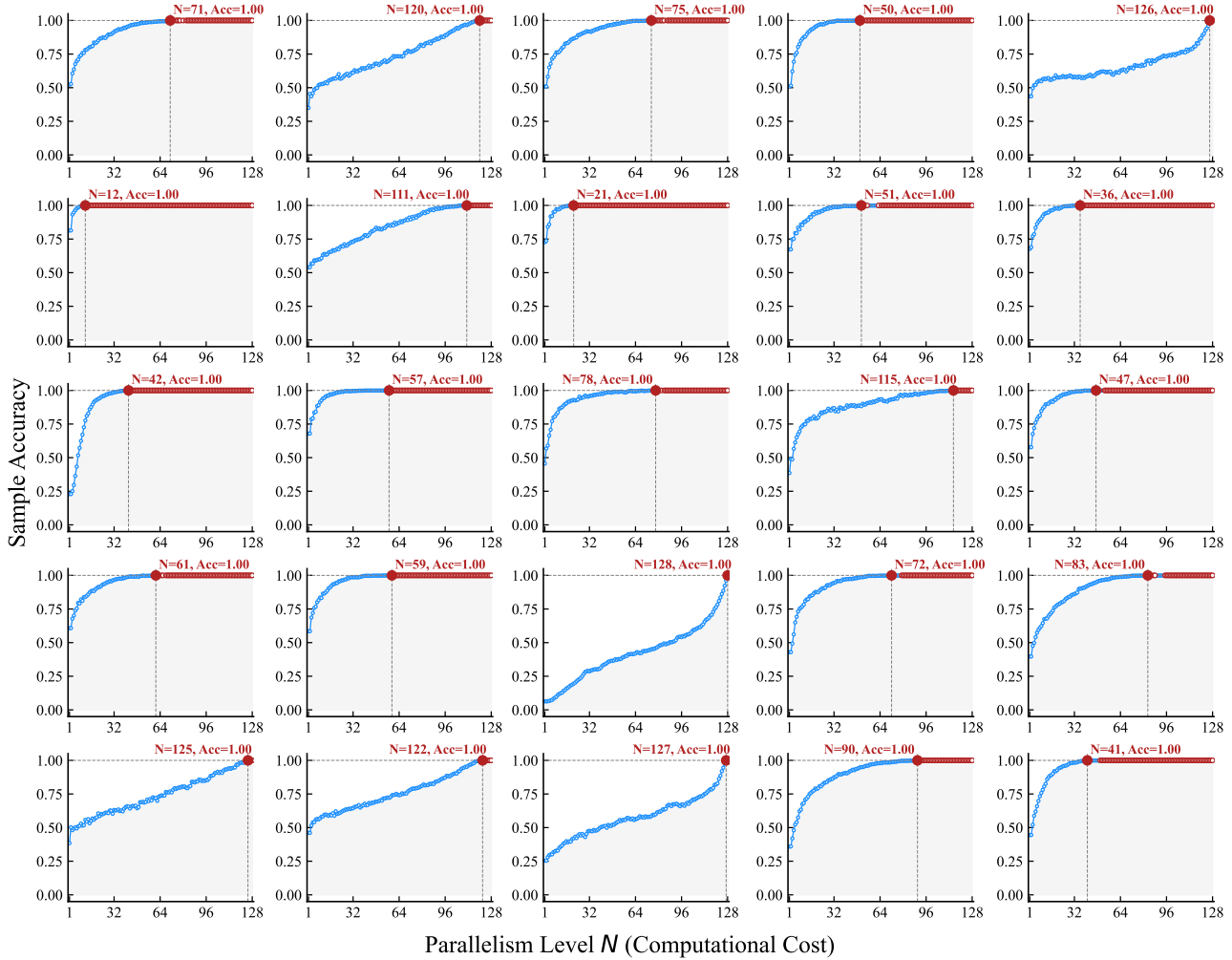


Figure 7. Examples of the “cost-accuracy” function $A_x(N)$ for **Type-(4)** samples from Qwen2.5-7B on the MATH500 dataset.

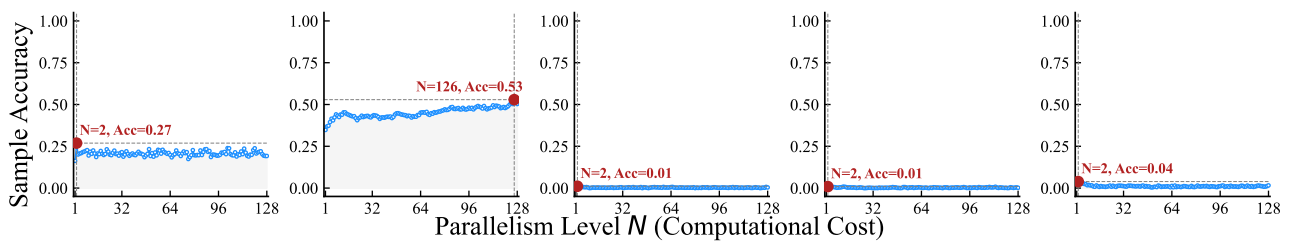


Figure 8. Examples of the “cost-accuracy” function $A_x(N)$ for **Type-(5)** samples from Qwen2.5-7B on the MATH500 dataset.

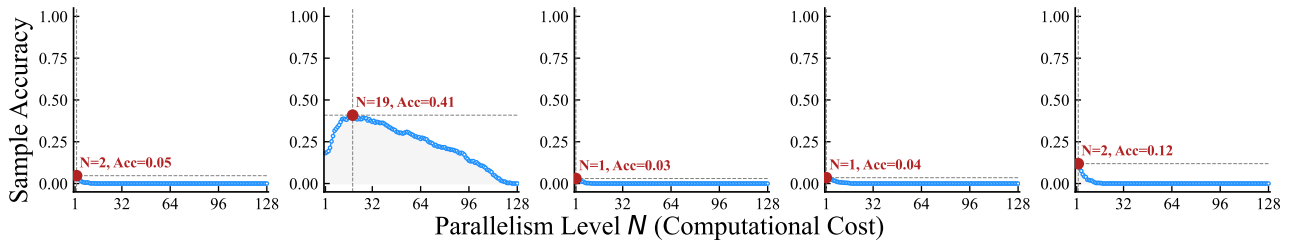


Figure 9. Examples of the “cost-accuracy” function $A_x(N)$ for **Type-(3)** samples from Qwen2.5-7B on the AIME24 dataset.

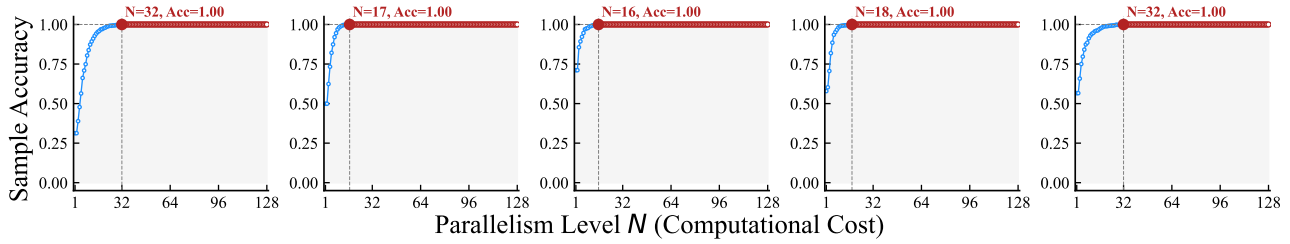


Figure 10. Examples of the “cost-accuracy” function $A_{\mathfrak{x}}(N)$ for **Type-(4)** samples from Qwen2.5-7B on the AIME24 dataset.

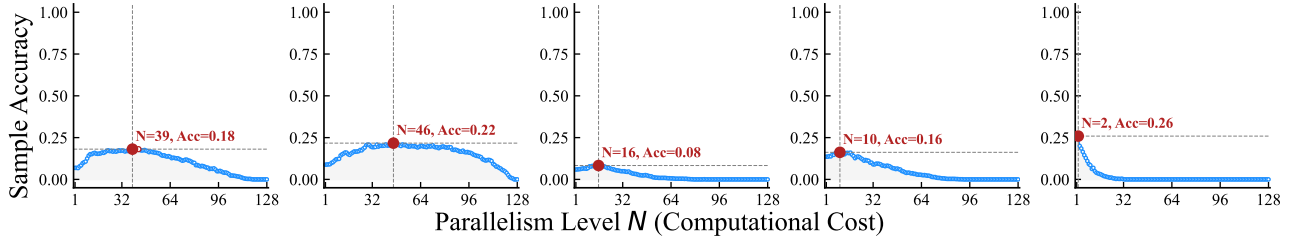


Figure 11. Examples of the “cost-accuracy” function $A_{\mathfrak{x}}(N)$ for **Type-(3)** samples from Qwen2.5-7B on the AIME25 dataset.

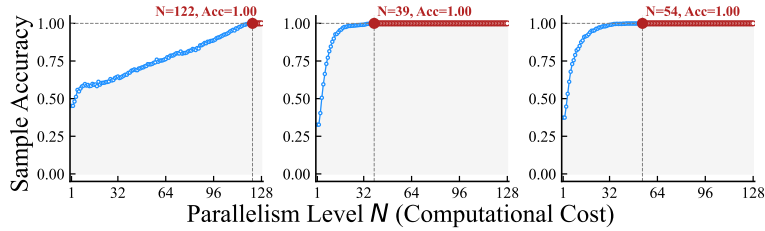


Figure 12. Examples of the “cost-accuracy” function $A_{\mathfrak{x}}(N)$ for **Type-(4)** samples from Qwen2.5-7B on the AIME25 dataset.

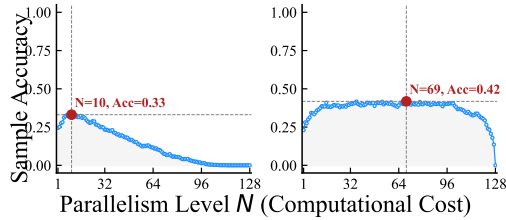


Figure 13. Examples of the “cost-accuracy” function $A_{\mathfrak{x}}(N)$ for **Type-(3)** samples from Qwen3-4B on the AIME24 dataset.

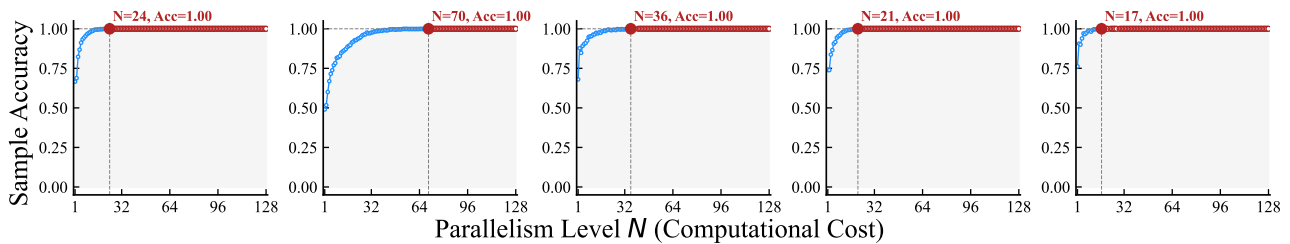


Figure 14. Examples of the “cost-accuracy” function $A_{\mathfrak{x}}(N)$ for **Type-(4)** samples from Qwen3-4B on the AIME24 dataset.

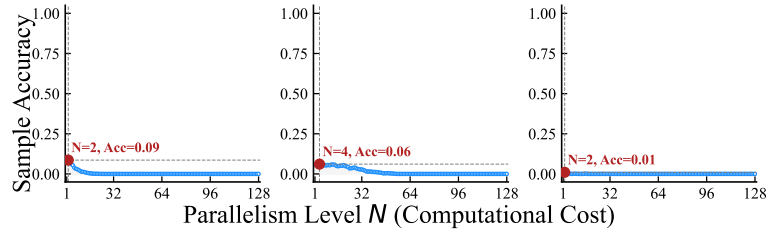


Figure 15. Examples of the “cost-accuracy” function $A_{\mathbf{x}}(N)$ for **Type-(3)** samples from Qwen3-4B on the AIME25 dataset.

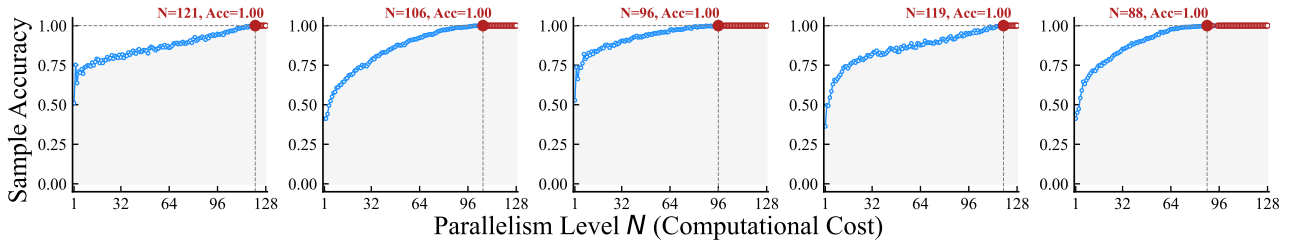


Figure 16. Examples of the “cost-accuracy” function $A_{\mathbf{x}}(N)$ for **Type-(4)** samples from Qwen3-4B on the AIME25 dataset.

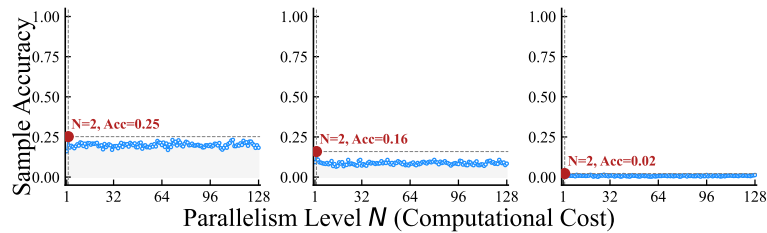


Figure 17. Examples of the “cost-accuracy” function $A_{\mathbf{x}}(N)$ for **Type-(5)** samples from Qwen3-4B on the AIME25 dataset.

C.2. Full Feature Distributions of Sample Types

[▷ Back to Table 2](#)

 Table 6. $N_{\mathcal{D}_i}^*$ and $\Delta_{\mathcal{D}_i}$ of each subset \mathcal{D}_i across datasets \mathcal{D} for Qwen2.5-7B.

\mathcal{D}	$N_{\mathcal{D}_i}^*$					$\Delta_{\mathcal{D}_i}(1, N_{\mathcal{D}_4}^*)$					$\Delta_{\mathcal{D}_i}(N_{\mathcal{D}_4}^*, N_{\max})$				
	(1)	(2)	(3)	(4)	(5)	(1)	(2)	(3)	(4)	(5)	(1)	(2)	(3)	(4)	(5)
MATH500	1.0	1.0	3.1	66.7	14.6	0.0	0.0	-0.08	0.24	0.03	0.0	0.0	-0.02	0.05	0.00
AMC	1.0	1.0	3.9	54.2	12.5	0.0	0.0	-0.11	0.32	-0.06	0.0	0.0	0.00	0.04	-0.01
AIME24	1.0	1.0	3.2	18.7	-	0.0	0.0	-0.04	0.43	-	0.0	0.0	0.00	0.05	-
AIME25	1.0	1.0	5.0	40.7	8.2	0.0	0.0	-0.09	0.56	0.07	0.0	0.0	-0.03	0.08	0.02
GPQA	1.0	1.0	6.5	62.7	13.3	0.0	0.0	-0.09	0.41	0.02	0.0	0.0	-0.03	0.06	0.00
MMLU-Pro	1.0	1.0	2.5	44.1	10.4	0.0	0.0	-0.14	0.35	-0.03	0.0	0.0	-0.04	0.07	-0.02

 Table 7. $N_{\mathcal{D}_i}^*$ and $\Delta_{\mathcal{D}_i}$ of each subset \mathcal{D}_i across datasets \mathcal{D} for Llama3.1-8B.

\mathcal{D}	$N_{\mathcal{D}_i}^*$					$\Delta_{\mathcal{D}_i}(1, N_{\mathcal{D}_4}^*)$					$\Delta_{\mathcal{D}_i}(N_{\mathcal{D}_4}^*, N_{\max})$				
	(1)	(2)	(3)	(4)	(5)	(1)	(2)	(3)	(4)	(5)	(1)	(2)	(3)	(4)	(5)
MATH500	1.0	1.0	3.2	48.9	15.4	0.0	0.0	-0.12	0.31	0.04	0.0	0.0	-0.03	0.04	0.00
AMC	1.0	1.0	2.8	74.7	11.2	0.0	0.0	-0.04	0.46	0.02	0.0	0.0	-0.03	0.04	0.00
AIME24	1.0	1.0	1.4	61.0	14.8	0.0	0.0	-0.03	0.60	0.12	0.0	0.0	-0.01	0.07	0.00
AIME25	1.0	1.0	2.4	37.6	13.5	0.0	0.0	-0.06	0.43	-0.04	0.0	0.0	-0.02	0.06	-0.03
GPQA	1.0	1.0	3.5	34.5	13.2	0.0	0.0	-0.07	0.50	0.08	0.0	0.0	-0.03	0.05	-0.03
MMLU-Pro	1.0	1.0	2.1	40.3	9.4	0.0	0.0	-0.14	0.38	-0.03	0.0	0.0	-0.04	0.10	0.00

 Table 8. $N_{\mathcal{D}_i}^*$ and $\Delta_{\mathcal{D}_i}$ of each subset \mathcal{D}_i across datasets \mathcal{D} for Deepseek-R1-Distill-Qwen-7B.

\mathcal{D}	$N_{\mathcal{D}_i}^*$					$\Delta_{\mathcal{D}_i}(1, N_{\mathcal{D}_4}^*)$					$\Delta_{\mathcal{D}_i}(N_{\mathcal{D}_4}^*, N_{\max})$				
	(1)	(2)	(3)	(4)	(5)	(1)	(2)	(3)	(4)	(5)	(1)	(2)	(3)	(4)	(5)
MATH500	1.0	1.0	3.4	33.2	13.9	0.0	0.0	-0.07	0.27	0.04	0.0	0.0	-0.03	0.07	0.01
AMC	1.0	1.0	4.2	57.8	11.8	0.0	0.0	-0.10	0.29	-0.05	0.0	0.0	-0.01	0.07	-0.02
AIME24	1.0	1.0	3.6	44.4	14.4	0.0	0.0	-0.05	0.39	0.05	0.0	0.0	-0.01	0.03	0.02
AIME25	1.0	1.0	5.4	83.9	9.6	0.0	0.0	-0.08	0.52	0.05	0.0	0.0	-0.04	0.07	0.01
GPQA	1.0	1.0	6.1	39.4	12.1	0.0	0.0	-0.11	0.44	0.03	0.0	0.0	0.00	0.05	0.00
MMLU-Pro	1.0	1.0	2.9	77.6	9.8	0.0	0.0	-0.13	0.38	-0.01	0.0	0.0	0.00	0.06	-0.01

C.3. Full Proportions of Sample Types

[▷ Back to Figure 4](#)

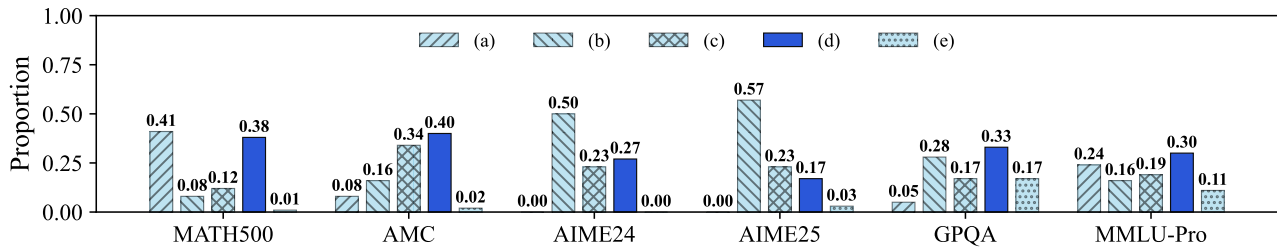


Figure 18. Proportion of the five sample types across datasets in Qwen2.5-7B.

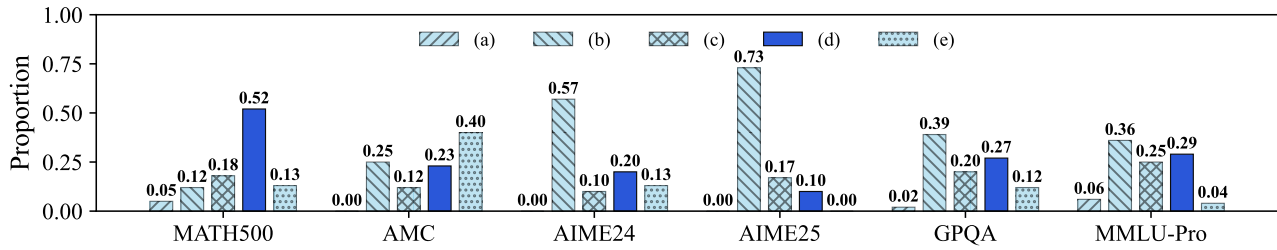


Figure 19. Proportion of the five sample types across datasets in Llama3.1-8B.

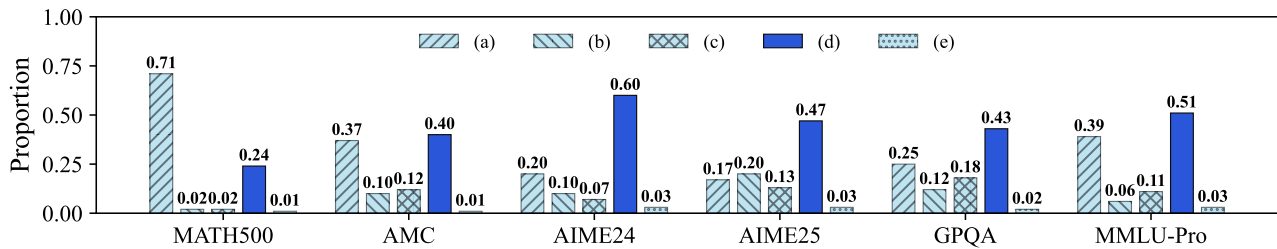


Figure 20. Proportion of the five sample types across datasets in Deepseek-R1-Distill-Qwen-7B.

D. Language Models

▷ [Back to Section 2.2](#)

Table 9 presents the detailed information of all language models used in this paper, including model paradigms, citations of the technique reports, and URL source links.

Table 9. Basic information of all language models used in this paper.

Model Name	Paradigm	Citation	URL Source
Llama3.1-8B	Non-Reasoning	(Grattafiori et al., 2024)	https://huggingface.co/meta-llama/Llama-3.1-8B-Instruct
Qwen2.5-7B	Non-Reasoning	(Yang et al., 2024)	https://huggingface.co/Qwen/Qwen2.5-7B-Instruct
R1-Distill-Qwen-7B	Reasoning	(Guo et al., 2025)	https://huggingface.co/deepseek-ai/DeepSeek-R1-Distill-Qwen-7B
Qwen3-4B	Non-Reasoning & Reasoning	(Yang et al., 2025a)	https://huggingface.co/Qwen/Qwen3-4B-Instruct-2507

E. Estimator Training

▷ [Back to Section 4.1](#)

Table 10 presents the training hyperparameters of all estimators.

Table 10. Training hyperparameters of all estimators.

Training Data Size	5000
Batch Size	128
Epoch	300
Learning Rate	1e-3
Weight Decay	1e-4
Optimizer	AdamW

Since DeepMath-103K contains ten progressively increasing difficulty levels, we uniformly allocate the training data across these levels, with 500 samples per difficulty. In addition, we also ensure that all five sample types are represented in the training set to avoid imbalance. Given that the inherent distribution of the five types is uneven, we enforce a minimum proportion of 12% for each type in the training data (with relatively fewer type-(3) and type-(5) samples and a higher proportion of type-(4) in practice), while not imposing further constraints on the exact proportions.

In addition, the validation set matches the training set in both size and sampling strategy, and is used for layer-wise weight estimation (Section 4.2).

F. Evaluation Setup

F.1. Baselines

▷ [Back to Section 5.1](#)

AC (Aggarwal et al., 2023). Adaptive-Consistency (AC) introduces a Beta Stopping Criteria. For each input, **AC samples outputs one by one** and performs an early-stopping check after each sampling. Suppose that n outputs have been sampled so far, yielding m distinct results with an distribution (p_1, p_2, \dots, p_m) , where $p_1 \geq p_2 \geq \dots \geq p_m$. If the condition $P(p_1 > p_2) \approx \int_0^{0.5} p_2^{v_2} \cdot (1 - p_2)^{v_1} dp_2 > 0.95$ is satisfied, sampling stops and the result corresponding to p_1 is returned as the final answer; otherwise, sampling continues until the maximum budget L is reached. In the original paper, $L = 40$, and we adopt the same settings in our implementation.

ESC (Li et al., 2024). Early-Stopping Self-Consistency (ESC) adopts a sliding-window entropy mechanism for adaptive early stopping. Specifically, for each input, **ESC samples w outputs in parallel at each step, where w denotes the window size**. If all outputs within the current window are identical, sampling terminates and this output is returned as the final

answer. Otherwise, ESC continues to sample another w outputs until reaching the maximum budget L , after which the most frequent output is selected as the final answer. In the original paper, $w = 8$ and $L = 64$ are used for MATH500, while $w = 5$ and $L = 40$ are used for other datasets. We adopt the same settings in our implementation.

DSC (Wang et al., 2025a). Difficulty-Adaptive Self-Consistency (DSC) follows a three-stage procedure. In Stage 1, the model ranks questions by estimating difficulty. In Stage 2, it processes questions from hardest to easiest and draws w samples per question. If k consecutive questions are encountered for which all w samples agree, it stops this pass and sets the sampling budget of all remaining (easier) questions to 1. In Stage 3, using the stopping point as a threshold, DSC draws one sample for each easier question, while for harder questions it adaptively increases the budget by doubling the number of w -sample blocks, up to a maximum of L samples. In the original paper, $w = 4$, $k = 32$, and $L = 40$. We adopt the same settings in our implementation.

DeepConf (Fu et al., 2025). Deep Think with Confidence (DeepConf) includes both offline and online algorithms; we mainly compare with its **online** variant, which belongs to efficient paradigms. The online algorithm consists of two stages. First, an *offline warm-up* stage **samples N_{init} outputs in parallel** to compute a trace confidence threshold s . Then, in the *adaptive sampling* stage, **outputs are sampled one by one**. During each sampling, a confidence check is performed every n tokens: if the trace confidence within a window falls below s , the current trace is truncated and a new sampling begins; otherwise, sampling continues until completion. After completing this sampling, trace-confidence-weighted majority voting is conducted over all collected outputs so far. If the highest frequency exceeds a threshold τ , sampling stops and that output is returned as the final answer; otherwise, sampling continues until reaching the maximum budget L . We set $N_{\text{init}} = 16$, $\tau = 0.95$, and $L = 512$ as in the original paper.

F.2. Computational Cost Calculation

▷ **Back to Section 5.1**

We measure computational cost in two dimensions: *memory overhead* and *inference latency*. For each model-dataset pair, we use *Std-PT*. as the baseline, and compute cost ratios as follows:

- *Memory Overhead* C_{mem} : Let M_w denote the GPU memory footprint of the LLM weights, and M_{kv} denote the peak KV-cache memory overhead during inference. For our method, we additionally introduce an estimator with memory overhead M_{est} . Let $M_{\text{kv}}^{\text{Std}}$ denote the peak KV-cache overhead of *Std-PT*. Then the average memory cost per sample (as a ratio to *Std-PT*.) is

$$C_{\text{mem}} := \begin{cases} \frac{M_w + M_{\text{kv}} + M_{\text{est}}}{M_w + M_{\text{kv}}^{\text{Std}}}, & \text{Our Method,} \\ \frac{M_w + M_{\text{kv}}}{M_w + M_{\text{kv}}^{\text{Std}}}, & \text{Other Methods.} \end{cases} \quad (71)$$

- *Inference Latency* C_{time} : Let T_{dec} denote the wall-clock decoding time, and T_{misc} denote the wall-clock time of all non-decoding operations. Here, T_{misc} includes (but is not limited to) estimator inference in our method and LLM-based difficulty ranking in DSC. Let $T_{\text{dec}}^{\text{Std}}$ denote the decoding time for *Std-PT*. We define the inference latency ratio (to *Std-PT*.) as

$$C_{\text{time}} := \frac{T_{\text{dec}} + T_{\text{misc}}}{T_{\text{dec}}^{\text{Std}}}. \quad (72)$$

G. More Experimental Results

G.1. Standard Deviations of Main Results

[▷ Back to Table 3](#)

Table 11 reports the standard deviations of accuracy (*Acc.*) of each method, model, and dataset.

Table 11. Standard deviation of accuracy (*Acc.*) across 32 runs.

Method	MATH500	AMC	AIME24	AIME25	GPQA	MMLU-Pro
Qwen2.5-7B						
Std-PT.	0.42	0.51	0.68	0.64	0.55	0.49
AC	0.63	0.71	0.89	0.82	0.74	0.66
ESC	0.58	0.65	0.76	0.73	0.61	0.59
DSC	0.61	0.69	0.83	0.79	0.70	0.68
DeepConf	0.77	0.84	1.02	0.96	0.88	0.91
T2 (Ours)	0.31	0.35	0.44	0.41	0.37	0.33
Llama3.1-8B						
Std-PT.	0.46	0.53	0.72	0.69	0.57	0.52
AC	0.68	0.76	0.95	0.91	0.79	0.74
ESC	0.61	0.70	0.84	0.81	0.66	0.63
DSC	0.65	0.73	0.88	0.85	0.71	0.69
DeepConf	0.82	0.91	1.10	1.05	0.93	0.97
T2 (Ours)	0.34	0.39	0.48	0.45	0.40	0.36
Deepseek-R1-Distill-Qwen-7B						
Std-PT.	0.38	0.44	0.59	0.56	0.47	0.45
AC	0.55	0.63	0.78	0.74	0.66	0.61
ESC	0.49	0.56	0.71	0.68	0.58	0.55
DSC	0.57	0.65	0.82	0.79	0.69	0.66
DeepConf	0.73	0.81	0.97	0.93	0.85	0.88
T2 (Ours)	0.26	0.30	0.38	0.36	0.31	0.29
Qwen3-4B						
Std-PT.	0.35	0.41	0.54	0.52	0.45	0.43
AC	0.51	0.60	0.73	0.71	0.63	0.59
ESC	0.47	0.55	0.68	0.66	0.57	0.54
DSC	0.53	0.61	0.75	0.72	0.64	0.60
DeepConf	0.69	0.78	0.92	0.89	0.81	0.84
T2 (Ours)	0.24	0.28	0.36	0.34	0.29	0.27

G.2. Detailed Inference Latency

[▷ Back to Section 5.2](#)

Table 12 reports the inference latency of our estimator. Since it depends solely on the hidden size of the applied language model, we report results on four different models.

Table 13 reports the average per-sample inference latency of each method for every model-dataset pair, including the time spent on all non-decoding operations.

Table 12. Inference latency of the estimator in T2.

Qwen2.5-7B	Llama3.1-8B	Deepseek-R1-Distill-Qwen-7B	Qwen3-4B
0.023ms	0.029ms	0.025ms	0.031ms

Table 13. Inference latency (seconds) of all methods.

	MATH500	AMC	AIME24	AIME25	GPQA	MMLU-Pro
Qwen2.5-7B						
<i>Std-PT.</i>	3.4	5.2	31.2	26.3	9.3	8.5
AC	5.1	12.1	108.0	74.4	25.1	17.3
ESC	9.4	9.9	30.0	38.1	21.1	15.1
DSC	4.9	11.2	57.1	25.5	20.3	31.8
DeepConf	11.7	13.9	98.6	49.4	31.7	27.3
T2 (Ours)	1.6	2.3	25.6	17.9	4.7	3.3
Llama3.1-8B						
<i>Std-PT.</i>	3.0	4.6	28.3	27.3	7.2	8.9
AC	5.1	10.4	100.7	95.6	21.5	28.2
ESC	4.2	9.3	46.4	66.6	17.1	19.2
DSC	5.2	10.0	46.1	26.8	15.0	25.2
DeepConf	7.1	12.0	113.8	142.5	30.0	37.0
T2 (Ours)	1.2	1.7	12.2	14.2	2.7	3.7
Deepseek-R1-Distill-Qwen-7B						
<i>Std-PT.</i>	15.7	24.2	204.9	225.4	72.1	64.7
AC	29.7	67.0	512.2	619.8	188.9	150.1
ESC	13.2	41.6	448.7	493.6	120.4	124.2
DSC	33.4	69.9	733.5	450.8	290.6	115.8
DeepConf	60.6	86.2	1020.4	804.7	274.0	251.0
T2 (Ours)	5.8	11.6	145.5	112.7	32.4	31.7
Qwen3-4B						
<i>Std-PT.</i>	6.5	11.1	65.3	51.4	33.2	30.7
AC	10.1	29.6	203.7	123.9	70.1	72.5
ESC	5.7	20.4	126.0	115.6	65.4	68.5
DSC	8.8	19.0	144.3	142.9	130.1	91.2
DeepConf	18.0	36.3	302.3	193.3	106.2	153.2
T2 (Ours)	2.9	5.8	51.6	28.8	15.3	12.3

G.3. Estimator Ablation

▷ [Back to Section 5.5](#)

Architecture. The only hyperparameter in the estimator architecture is the MLP hidden size, which we set to $\lfloor rd \rfloor$ with $r = 1/8$, where d is the language model’s hidden dimension. We vary r to study the effect of hidden size on T2’s performance. [Figure 21](#) and [22](#) show the results on MATH500 and AIME25. When $r < 1/8$, performance degrades to different extents across models; when $r > 1/8$, performance largely saturates, suggesting that the estimator capacity is already sufficient for the task and further scaling brings little benefit.

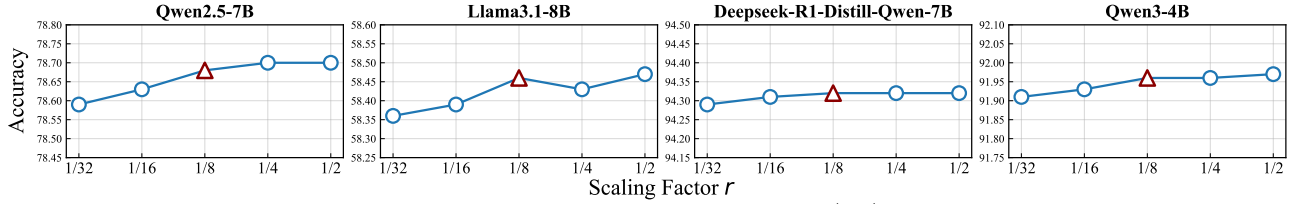


Figure 21. Results under varying scaling factor r of MLP hidden size $\lfloor rd \rfloor$ on the MATH500 dataset.

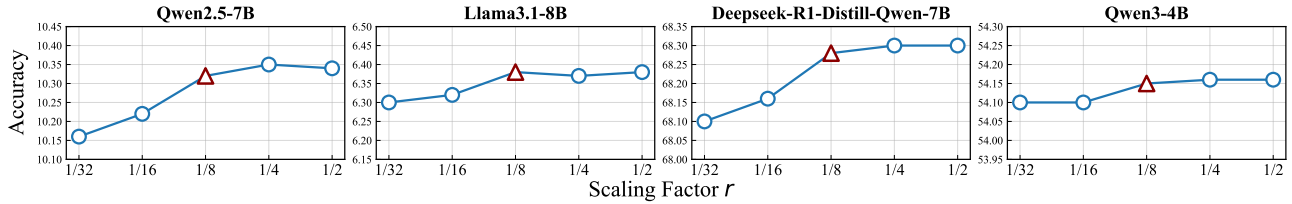


Figure 22. Results under varying scaling factor r of MLP hidden size $\lfloor rd \rfloor$ on the AIME25 dataset.

Training Data Size. We also study the effect of the estimator’s training data size. In our main experiments, the estimator is trained on 5k samples; we vary this size to evaluate its effect on T2’s performance. [Figure 23](#) and [24](#) show the ablation results on MATH500 and AIME25. Overall, performance gains after 5k samples slow down noticeably compared with earlier scaling, and mild overfitting is even observed at 10k for Qwen. Therefore, 5k is the most balanced training size.

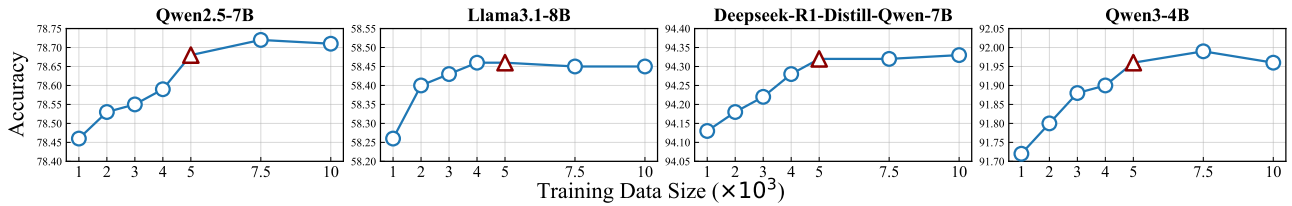


Figure 23. Results under varying training data sizes for estimators on the MATH500 dataset.

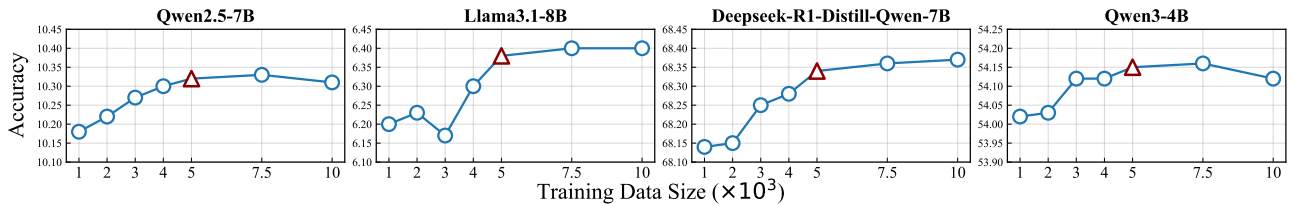


Figure 24. Results under varying training data sizes for estimators on the AIME25 dataset.